

Asymmetric organelle positioning during epithelial polarization of *C. elegans* intestinal cells

James N. Brandt¹, Laura Voss¹, Fiona M. Rambo, Katelyn Nicholson, Jackson R. Thein, Lydia Fairchild, Laurence Seabrook, Danielia Lewis, Lali Guevara-Hernandez, Matthew L. White, Luca Sax, Victoria Eichten, Logan Harper, Greg J. Hermann^{*}

Department of Biology, Lewis & Clark College, Portland, OR, USA



ARTICLE INFO

Keywords:
Epithelial polarization
Organelle positioning
ABC transporter
Rab GTPase
C. elegans

ABSTRACT

While the epithelial cell cortex displays profound asymmetries in protein distribution and morphology along the apico-basal axis, the extent to which the cytoplasm is similarly polarized within epithelial cells remains relatively unexplored. We show that cytoplasmic organelles within *C. elegans* embryonic intestinal cells develop extensive apico-basal polarity at the time they establish cortical asymmetry. Nuclei and conventional endosomes, including early endosomes, late endosomes, and lysosomes, become polarized apically. Lysosome-related gut granules, yolk platelets, and lipid droplets become basally enriched. Removal of *par-3* activity does not disrupt organelle positioning, indicating that cytoplasmic apico-basal asymmetry is independent of the PAR polarity pathway. Blocking the apical migration of nuclei leads to the apical positioning of gut granules and yolk platelets, whereas the asymmetric localization of conventional endosomes and lipid droplets is unaltered. This suggests that nuclear positioning organizes some, but not all, cytoplasmic asymmetries in this cell type. We show that gut granules become apically enriched when *WHT-2* and *WHT-7* function is disrupted, identifying a novel role for ABCG transporters in gut granule positioning during epithelial polarization. Analysis of *WHT-2* and *WHT-7* ATPase mutants is consistent with a *WHT-2*/*WHT-7* heterodimer acting as a transporter in gut granule positioning. In *wht-2*(*–*) mutants, the polarized distribution of other organelles is not altered and gut granules do not take on characteristics of conventional endosomes that could have explained their apical mispositioning. During epithelial polarization *wht-2*(*–*) gut granules exhibit a loss of the Rab32/38 family member *GLO-1* and ectopic expression of *GLO-1* is sufficient to rescue the basal positioning of *wht-2*(*–*) and *wht-7*(*–*) gut granules. Furthermore, depletion of *GLO-1* causes the mislocalization of the endolysosomal *RAB-7* to gut granules and *RAB-7* drives the apical mispositioning of gut granules when *GLO-1*, *WHT-2*, or *WHT-7* function is disrupted. We suggest that ABC transporters residing on gut granules can regulate Rab dynamics to control organelle positioning during epithelial polarization.

1. Introduction

The epithelial cells lining the interior and exterior surfaces of organs and tissues function as barriers, promote selective transport, and provide mechanical strength in embryos and mature organisms (Simons and Fuller, 1985). Epithelial cells characteristically segregate the cell cortex, including both the plasma membrane and underlying cytoplasm, into distinct apical, lateral, and basal domains (Pickett et al., 2019). The outward facing apical domain often harbors specialized structures such as microvilli or cilia, the lateral domain contacts other epithelial cells and

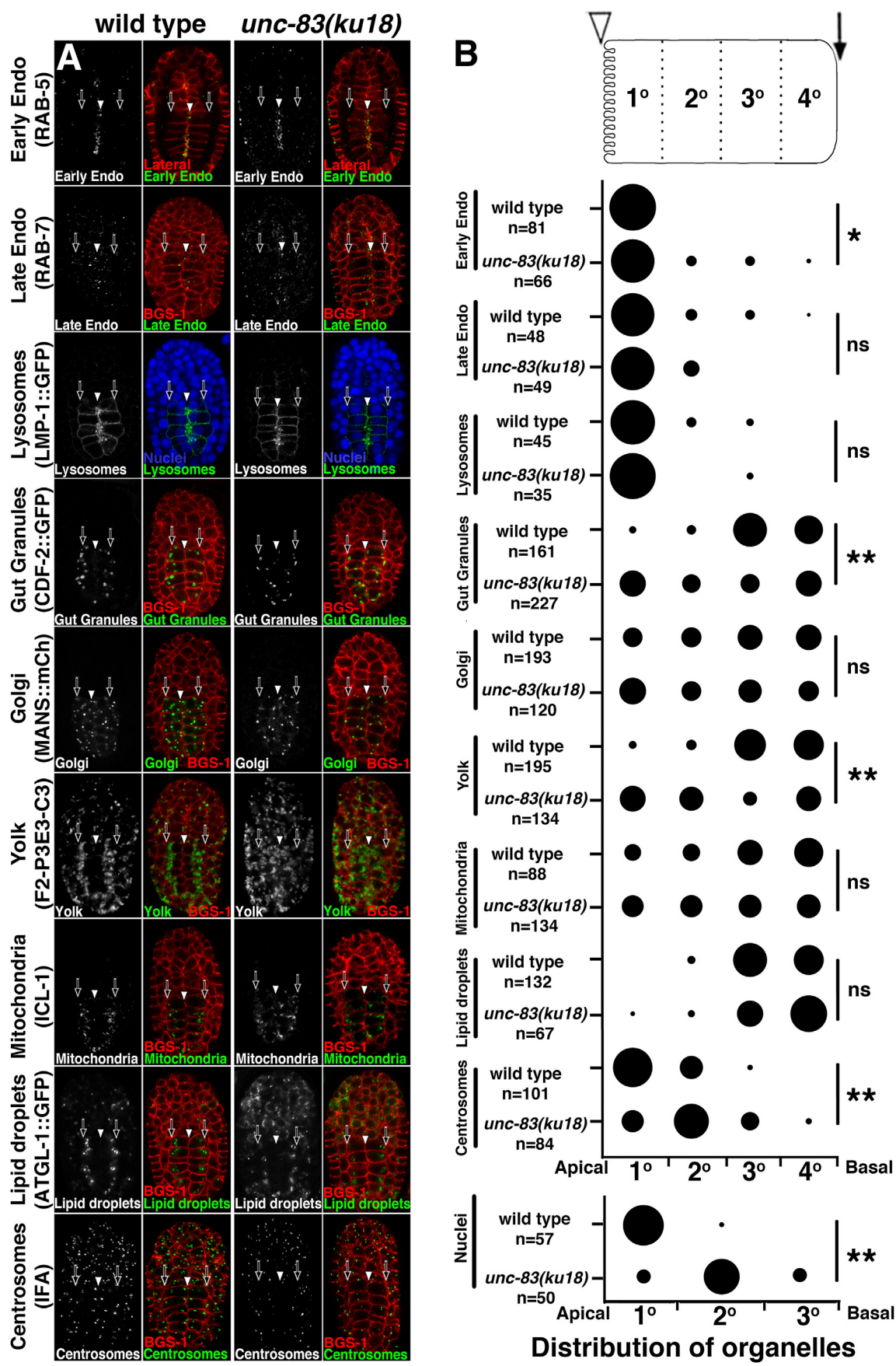
contains cell-cell junction complexes, and the basal domain opposes the apical domain, typically interacting with the extracellular matrix (Rodriguez-Boulan and Macara, 2014). Epithelial cells can also exhibit pronounced apico-basal polarity in the distribution of their cytoplasmic organelles, resulting in important physical and functional characteristics (Taverna et al., 2014; Roman-Fernandez and Bryant, 2016).

Well-studied and conserved PAR, CRB, and SCRB polarity complexes mediate the apico-basolateral polarization of the epithelial cell cortex (Pickett et al., 2019; Riga et al., 2020). These complexes collaborate with endosomal organelles to establish and maintain the selective trafficking

* Corresponding author. Department of Biology, Lewis & Clark College, Portland, OR, USA.

E-mail address: hermann@lclark.edu (G.J. Hermann).

¹ The authors contributed equally to the work.



(caption on next page)

Fig. 1. Organelles are asymmetrically positioned in polarizing intestinal epithelial cells. (A) Organelles in wild type or *unc-83(ku18)* E16 stage embryos were marked with antibodies or fluorescent proteins. To identify the apical and basal domains of intestinal cells at this stage, embryos were stained with a monoclonal antibody that labels the lateral domain of epithelial cells, antibodies to BGS-1, which labels the cell cortex, or DAPI to mark nuclei. Co-stained embryos were imaged with confocal microscopy. Single confocal optical sections acquired at the focal plane that contains the majority of intestinal nuclei are shown. The white arrowhead marks the midline/apical domain and the black arrows denote the basal domain of the intestinal cells. Embryos are 50 μ m in length and are oriented so that the anterior is at the top and the posterior is at the bottom of each panel. (B) To quantify organelle position, intestinal cells were divided into 3 or 4 equally sized quadrants along the apical basal axis. The number of organelles within each quadrant was scored. Only organelles present within the same focal plane as the nucleus were analyzed. The position of organelles within 8–12 individual intestinal cells was scored in 5–10 embryos of each genotype. The total number of organelles scored is listed below the genotype. In the graph, the area of the circle represents the proportion of organelles located within each quadrant. A Fisher's exact test followed by a Bonferroni correction was used to compare the distribution of each type of organelle between wild type and *unc-83(ku18)* (ns represents a $p > 0.05$, * represents a $p \leq 0.05$, and ** represents a $p \leq 0.001$).

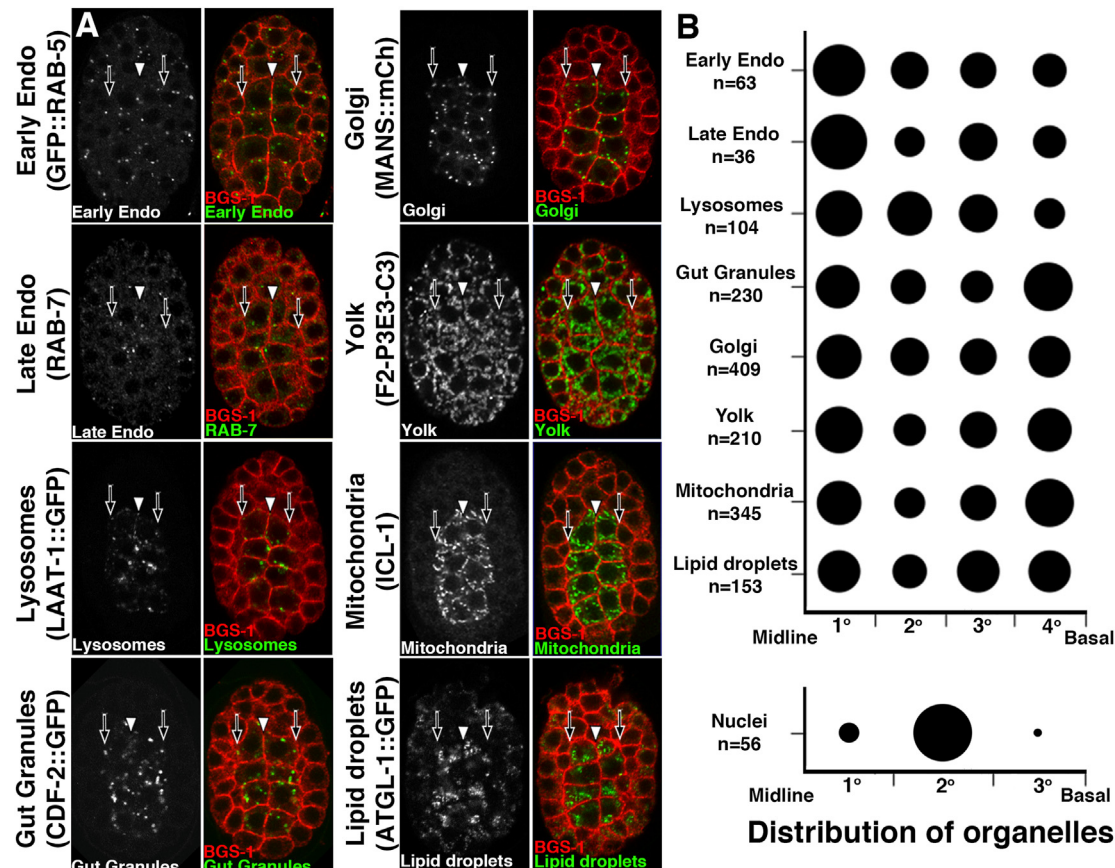


Fig. 2. Organelles are not asymmetrically positioned in intestinal cells prior to epithelial polarization. (A) Wild-type E8 stage embryos were stained with antibodies to the cortical protein BGS-1 and organelles were marked with GFP tagged proteins or antibodies. Embryos were imaged with confocal microscopy, single optical sections are shown, and white arrowheads and black arrows mark the midline and basal intestinal cell domains, respectively. (B) The position of organelles within individual intestinal cells was scored as described in the legend for Fig. 1. The area of the circles represents the proportion of organelles located within each quadrant.

of proteins to the apical or basolateral plasma membrane (Apodaca et al., 2012; Eaton and Martin-Belmonte, 2014; Mellman and Nelson, 2008). The polarity complexes also influence the localization of recycling endosomes normally associated with the apical domain of epithelial cells (Winter et al., 2012). For most epithelia, it remains an open question which organelles are asymmetrically positioned and whether the polarity complexes direct their segregation within the cytoplasm.

The polarization of intestinal epithelial cells has been extensively studied in *C. elegans* embryos (Pickett et al., 2019; Maduro, 2017). Midway through embryogenesis, two rows of intestinal cells rapidly polarize so that their apical surface faces a lumen positioned between the two sides of the bilaterally symmetric intestinal primordium (Leung et al., 1999). In these cells, the cortical PAR complex protein PAR-3 is both the most upstream regulator and first protein known to be asymmetrically localized during epithelial polarization (Achilleos et al., 2010). While the intestinal cell cortex is being segregated into apical and

basolateral domains, nuclei and centrioles become asymmetrically localized toward the apical domain whereas lysosome related organelles (LROs), called gut granules, become basally enriched (Leung et al., 1999; Achilleos et al., 2010; Starr et al., 2001; Hermann et al., 2005), suggesting that the cytoplasm becomes polarized during this time as well. At the end of embryogenesis, recycling endosomes, early endosomes, late endosomes, and lysosomes are enriched near the apical cortex (Hermann et al., 2005; Rabbitts et al., 2008; Zhang et al., 2011). In adults, recycling and early endosomes remain apically localized, whereas late endosomes and lysosomes are equally distributed along the apico-basal axis (Winter et al., 2012; Chen et al., 2006, 2010). It is currently not known whether the asymmetrical positioning of endosomal compartments is coordinated with epithelial polarization during embryogenesis.

Factors functioning in endosome biogenesis can also direct the intracellular movement and localization of endosomes (Ballabio and Bonifacino, 2020; Neefjes et al., 2017). For example, Rab5 labeled early

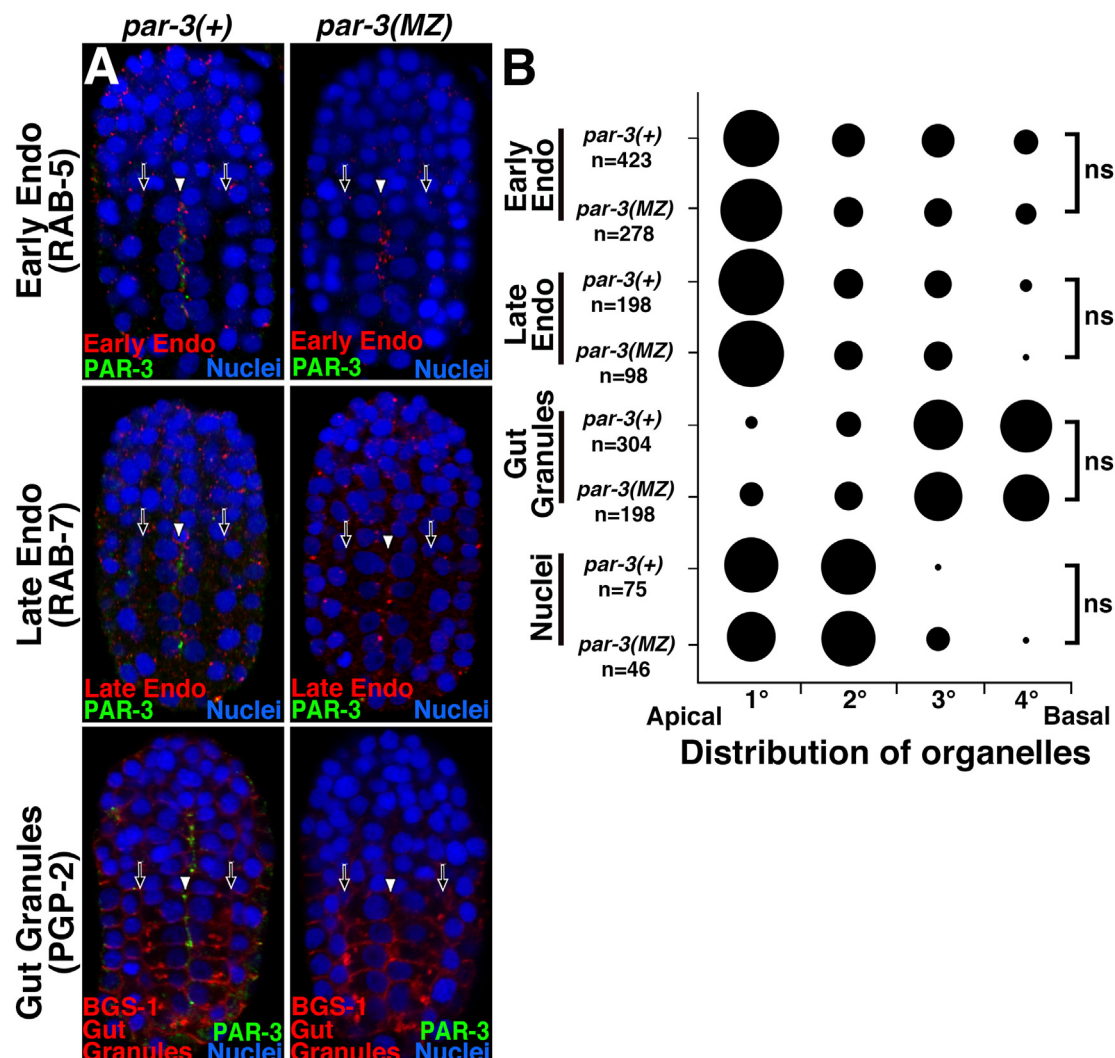


Fig. 3. Asymmetric organelle positioning does not require PAR-3. (A) Wild-type or *par-3(MZ)* E16 stage embryos were stained with the indicated antibodies and DAPI to mark nuclei and imaged with confocal microscopy. Single optical sections are shown, and white arrowheads and black arrows mark the apical and basal intestinal cell domains, respectively. (B) The position of organelles within individual intestinal cells was scored as described in the legend for Fig. 1. The area of the circles represents the proportion of organelles located within each quadrant. A Fisher's exact test was used to compare the distribution of each type of organelle between wild type and *par-3(MZ)* (ns represents a $p > 0.05$).

endosomes are transformed into late endosomes marked by Rab7, which directs the removal of specific cargo and their fusion with Arf labeled lysosomes (Khatter et al., 2015; Kummel and Ungermann, 2014; Scott et al., 2014; Trivedi et al., 2020). The same Rab and Arf GTPases that function in these endosomal protein trafficking events also mediate endosome, lysosome, and LRO motility by interacting with different sets of effectors (Ballabio and Bonifacino, 2020; Neefjes et al., 2017; Park et al., 2007). Whether other components of the endosomal protein trafficking machinery mediate endosomal positioning within cells has remained relatively unexplored.

In this work we describe the apico-basal polarization of a diverse collection of organelles during the polarization of *C. elegans* intestinal epithelial cells. We show that the cytoplasmic polarization of epithelial cells does not require PAR-3 and demonstrate that apically directed nuclear migration contributes to the asymmetric distribution of some but not all basal organelles. We identify the WHT-2 and WHT-7 ABCG transporters as a key factor required for the basal localization of LROs and we show that they likely impact LRO positioning through Rab activity (Voss et al., 2020).

2. Materials and methods

2.1. Mutations and strains

C. elegans strains were grown at 22 °C on NGM media seeded with OP50 *Escherichia coli* (Stiernagle, 1999). N2 was used as the wild-type strain and was the background used to create the following mutations that were used in this study: *apt-6(ok429)*, *glo-2(tm592)*, *glo-3(kx38)*, *par-3(tm2716)*, *rab-7(ok511)*, *unc-83(ku18)*, *vps-18(tm1125)*, *wht-1(tm688)*, *wht-2(ok2775)*, *wht-2(gk891224)*, *wht-3(ok927)*, *wht-4(ok1007)*, *wht-5(ok806)*, *wht-6(ok882)*, *wht-7(ok812)*, *wht-7(gk692424)*, *wht-8(ok3112)*. Descriptions of each mutant allele can be found at Wormbase (www.wormbase.org). The following CRISPR genome edited alleles were used: *glo-1(syb1102[gfp::glo-1])* (Voss et al., 2020), *wht-2(syb668[K74M])* (Voss et al., 2020), *wht-2(syb745[K74R])* (Voss et al., 2020), *wht-7(syb1988[K105M])* (this work), *wht-7(syb1982[K105R])* (this work). The following transgenes were used: *amIs4[cdf-2p::cdf-2::gfp::unc-119(+)]* (Davis et al., 2009), *hjIs67[atgl-1p::atgl-1::gfp; mec-7::rfp]* (Zhang et al., 2010), *kxEx9[glo-1p::gfp::glo-1(+)]*.

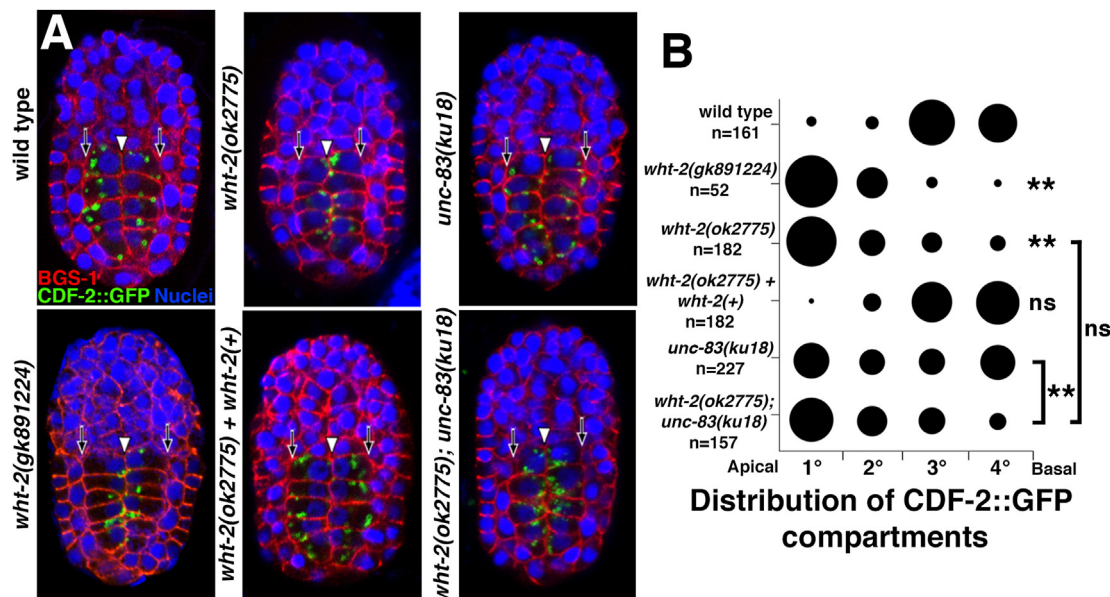


Fig. 4. CDF-2::GFP marked organelles are positioned apically rather than basally in *wht-2*($-$) mutants. E16 stage embryos expressing CDF-2::GFP were stained with BGS-1 to mark the cell cortex and DAPI to mark nuclei. Single optical sections are shown, and white arrowheads and black arrows mark the apical and basal intestinal cell domains, respectively. (B) The position of organelles within individual intestinal cells was scored as described in the legend for Fig. 1. The area of the circles represents the proportion of organelles located within each quadrant. A Fisher's exact test followed by a Bonferroni correction was used to compare the distribution of each type of organelle between the mutant and wild type unless otherwise noted (ns represents a $p > 0.05$ and ** represents a $p \leq 0.001$).

Rol-6^D (Hermann et al., 2005), *kxE*152[*asm-1p::asm-1::mCherry*; *Rol-6^D*] (Levitte et al., 2010), *kxE*230[*glo-1p::gfp::glo-1*(Q71L); *Rol-6^D*] (Morris et al., 2018), *kxE*231[*glo-1::gfp::glo-1*(T25N); *Rol-6^D*] (Morris et al., 2018), *kxE*287[*wht-2p::wht-2*(+); *Rol-6^D*] (Voss et al., 2020), *kxE*288[*WRM0639dG05*; *Rol-6^D*] (this work), *kxIs5*[*glo-1p::mans::mCherry*; *unc-119*(+)] (Voss et al., 2020), *ltSi910*[*elt-2p::vhvGFP4::zf-1::operon-linker::mCherry::his-11::tb2-2*; *unc-119*(+)] (Wang et al., 2017), *opIs222*[*eft-3p::gfp::fyve::fyve*; *unc-119*(+)] (Neukomm et al., 2011), *pwiIs20*[*pie-1p::gfp::rab-5*; *unc-119*(+)] (Sato et al., 2005), *pwiIs50*[*lmp-1p::lmp-1p::gfp*; *unc-119*(+)] (Treusch et al., 2004), *qxlIs354*[*ced-1p::laat-1::gfp*] (Liu et al., 2012), *tdEx2*[*arl-8p::arl-8::gfp*; *Rol-6^D*] (Nakae et al., 2010), *zulIs20*[*par-3p::par-3::zf1::gfp*; *unc-119*(+)] (Nance et al., 2003).

2.2. Genetic manipulations

wht-2(gk891224) was identified in a screen of Million Mutation strains for mispositioning of autofluorescent gut granules in E16 stage embryos. *wht-2(ok2775)* embryos showed the same defect in gut granule positioning, which was rescued by the presence of *kxE*287[*wht-2*(+)]. Both *wht-7(ok812)* and *wht-7(gk692424)* showed a similar defect in positioning of autofluorescent gut granules in E16 stage embryos. Gut granule positioning was restored in *wht-7(ok812)* embryos when the *wht-7*(+) containing fosmid *WRM0639dG05* was injected at 5 ng/ μ l with PRF4 at 100 ng/ μ l. The resulting *kxE*288 array was used to score rescue.

CRISPR-Cas9-mediated gene editing was carried out by SunyBiotech (Fuzhou, Fujian, China) to generate PHX1976 *wht-7(syb1976)* and PHX1988 *wht-7(syb1988)*, which precisely change lysine 105 to methionine, and PHX1982 *wht-7(syb1982)* and PHX2008 *wht-7(syb2008)*, which precisely change lysine 105 to arginine. The mutations were verified with Sanger DNA sequencing. The sequence of the first 65 nucleotides of exon four of the *wht-7* K105M and K105R mutations are shown:

K105M

TGTCGGAGTGGCTCGACCCGGAGAGGTTACgGCGATCATTGGgCC
CAGTGGAGCTGGcATGACT

K105R

TGTCGGAGTGGCTCGACCCGGAGAGGTTACgGCGATCATTGGgCC
CAGTGGAGCTGGcCGCACT

The underlined upper case nucleotides indicate the point mutations changing K105 and the underlined lower case nucleotides indicate the synonymous mutations that alter the sgRNA or protospacer adjacent motif to prevent recutting by CRISPR-Cas9. The positioning of gut granules was normal in the K105M and K105R alleles; *wht-7(syb1988* [K105M]) and *wht-7(syb1982*[K105R]) were used in this study.

wht-2(K74 M/R); *wht-7(K105 M/R)* double mutants were generated using *wht-2(K74 M/R)*; *wht-7(ok812)* deletion strains. These strains were created by mating *wht-7(ok812)* males with *wht-2(K74 M/R)* point mutants and isolating resulting lines that mislocalized autofluorescent gut granules apically in E16 stage embryos, indicating that *wht-7(ok812)* was homozygous, and that lacked birefringent gut granules at the 1.5-fold stage embryos, indicating that *wht-2(K74 M/R)* was present. The presence of the *wht-2* point mutation and *wht-7* deletion in these strains was verified by Sanger DNA sequencing (Genewiz, South Plainfield, NJ) and PCR, respectively. *wht-2(K74 M/R)*; *wht-7(ok812)* strains were then mated with *wht-2*(+); *wht-7(K105 M/R)* males and progeny were isolated that lacked birefringent granules in 1.5-fold stage embryos, indicating that *wht-2(K74 M/R)* was homozygous, and that lacked the *wht-7(ok812)* deletion scored with PCR, indicating *wht-7(K105 M/R)* was homozygous. The presence of the *wht-2* and *wht-7* point mutations in the resulting strains were verified by DNA sequencing.

Transgenes were typically moved into mutant backgrounds by crossing males carrying the mutation with hermaphrodites containing the transgene. Resulting strains were confirmed to contain the extrachromosomal array, be homozygous for the mutation, or be homozygous for the integrated transgene through phenotypic analysis. The *wht-2*(-); *unc-83(ku18)* double mutant was identified in progeny of a cross between the single mutants that displayed both the reduction of birefringent granules in pretzel stage embryos, which indicates homozygosity for *wht-2*(-) (Voss et al., 2020), and the lack of nuclear polarization in bean stage embryonic intestinal cells, which indicates homozygosity for *unc-83(ku18)* (Starr et al., 2001). The *wht-2(ok2775)* and *wht-7(ok812)*

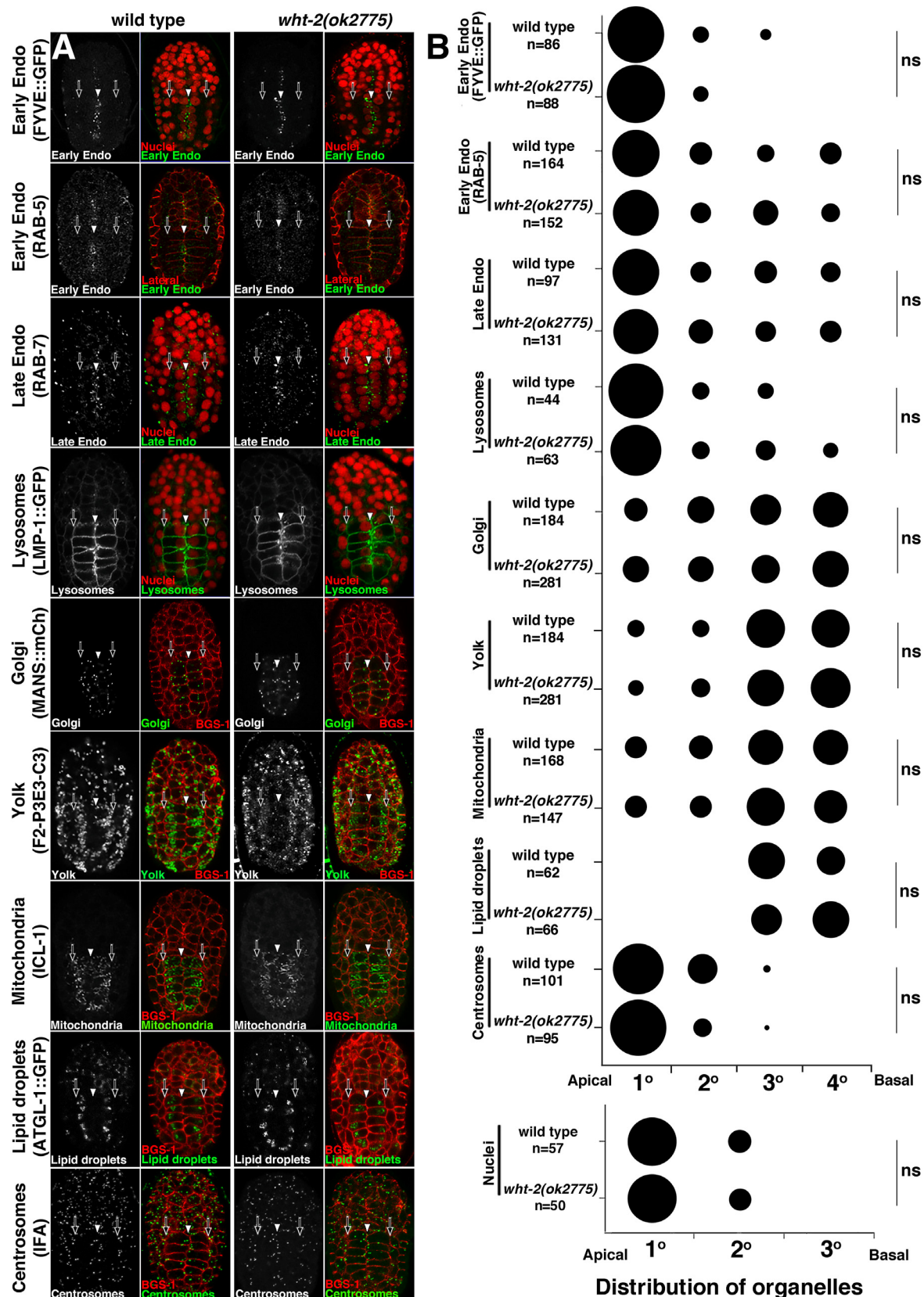


Fig. 5. Organelle positioning during epithelial polarization in *wht-2(–)* mutants. (A) Organelles in wild type or *wht-2(ok2775)* E16 stage embryos were marked with antibodies or fluorescent proteins. The apical and basal domain of intestinal cells was identified by labeling nuclei, the lateral domain, or the cell cortex. Single confocal optical sections are shown. The white arrowhead marks the apical domain and the black arrows denote the basal domain of the intestinal cells. (B) The position of organelles within individual intestinal cells was scored as described in the legend for Fig. 1. The area of the circles represents the proportion of organelles located within each quadrant. A Fisher's exact test followed by a Bonferroni correction was used to compare the distribution of each type of organelle between the *wht-2(–)* mutant and wild type (ns represents a $p > 0.05$).

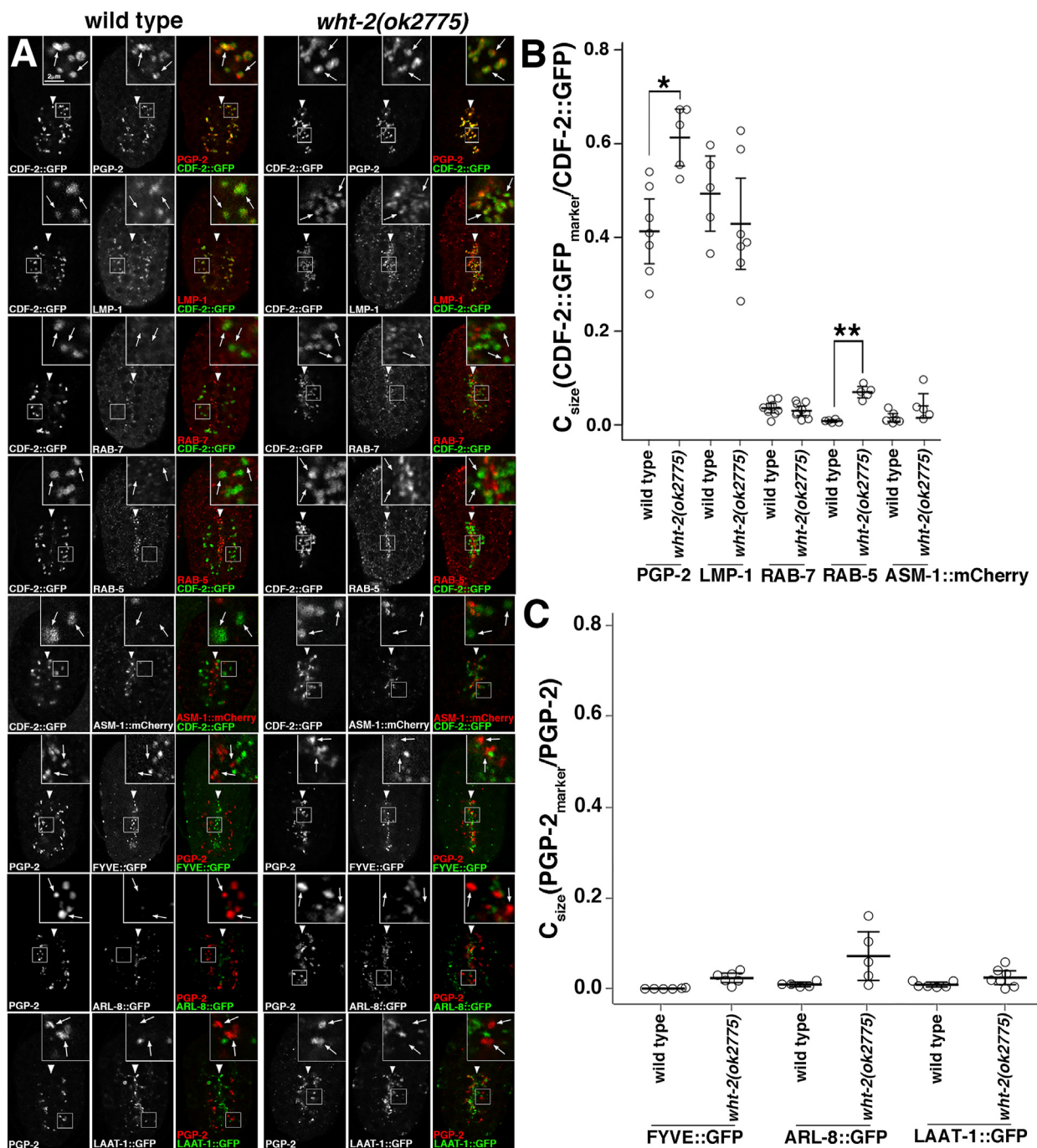


Fig. 6. Gut granule identity is not altered in *wht-2*(*-*) mutants. The localization of CDF-2::GFP or PGP-2 was assessed relative to gut granule or conventional endosomal markers in E16 stage embryos with confocal microscopy. In insets, white arrows denote compartments containing CDF-2::GFP or PGP-2. (B and C) SQUASH software was used to calculate C_{size} , which describes the proportion of the total CDF-2::GFP or PGP-2 area within an embryo that also contains the indicated marker. Five to ten embryos were analyzed. The mean is plotted and the error bars represent the 95% confidence limit. Wild type and *wht-2*(*-*) were compared to each other with a one-way ANOVA (* represents a $p \leq 0.05$, ** represents a $p \leq 0.001$, and all others $p > 0.05$).

double mutants with *glo-3(kx38)* were identified by isolating progeny of a cross between the single mutants that displayed reduced numbers of enlarged birefringent gut granules in pretzel stage embryos, which indicates homozygosity for *glo-3(kx38)* (Morris et al., 2018), and that were also homozygous for the *wht* deletion shown by PCR screening. The *wht-2(ok2775); wht-7(ok812)* double mutant was isolated in progeny of a cross between the single mutants that showed a reduction in birefringent gut granules, which indicates homozygosity for *wht-2(ok1775)* (Voss et al., 2020), that were also homozygous for the *wht-7(ok812)* deletion shown by PCR screening. The *ltSi910[intDEG]*; *glo-1(syb1102[gfp::glo-1])*

double mutant was created by crossing *glo-1(syb1102[gfp::glo-1])* with *ltSi910[intDEG]* and identifying a line that was homozygous for *glo-1(syb1102[gfp::glo-1])* and heterozygous for *ltSi910[intDEG]*, which was shown by its E16 stage progeny always exhibiting GFP::GLO-1 expression except in embryos that expressed mCherry::HIS-11 from *intDEG* (Wang et al., 2017).

par-3(MZ) embryos, which lack zygotic and maternally contributed *par-3* at the E16 stage, were generated using the strategy described in (Achilleos et al., 2010). *par-3(tm2716)*; *unc-32(e189)/qC1* [*dpy-19(e1259); him-8(e1489)*] males were mated with *par-3(tm2716)*

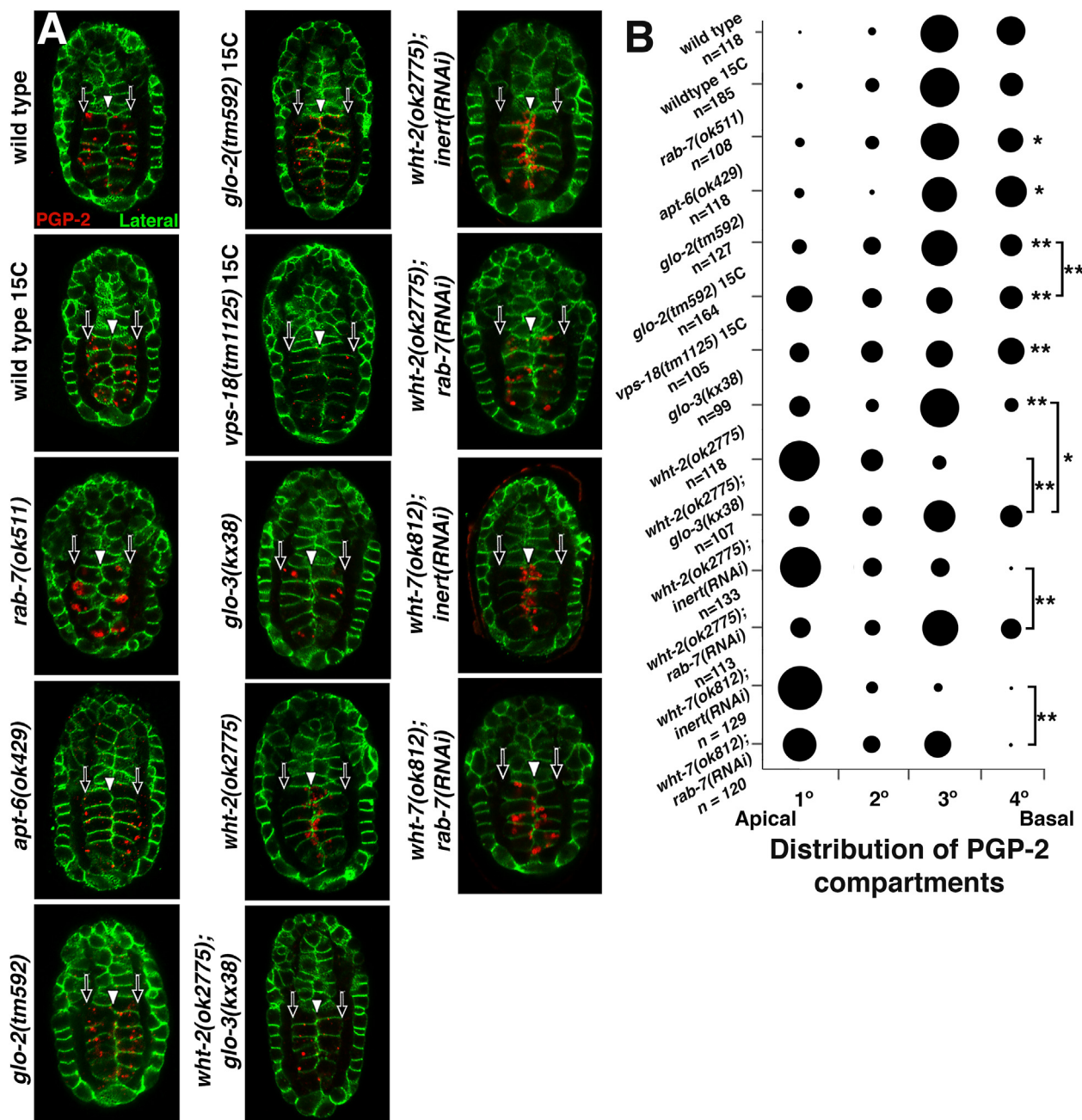


Fig. 7. Gut granule biogenesis mutants disrupt the positioning of PGP-2 marked organelles during epithelial polarization. (A) Wild-type or mutant E16 stage embryos were stained with antibodies marking PGP-2 and lateral domains and imaged with confocal microscopy. Single optical sections are shown, and white arrowheads and black arrows mark the apical and basal intestinal cell domains, respectively. Unless otherwise indicated all embryos were grown at 22C. (B) The position of organelles within individual intestinal cells was scored as described in the legend for Fig. 1. The area of the circles represents the proportion of organelles located within each quadrant. A Fisher's exact test followed by a Bonferroni correction was used to compare the distribution of PGP-2 compartment positioning in the mutants and wild type or as indicated by brackets (* represents a $p \leq 0.05$ and ** represents a $p \leq 0.001$).

unc-32(e189); zuis20[par-3::par-3::zf1::gfp; unc-119(+)] hermaphrodites. Typically 40 outcross *Unc* progeny, which are *par-3(tm2716)* *unc-32(e189)/par-3(tm2716)* *unc-32(e189); par-3::zf1::gfp/+*, were placed on a plate and allowed to self fertilize. The resulting embryos, $\frac{1}{4}$ of which are *par-3(MZ)*, were analyzed. *par-3(MZ)* embryos were identified in the population by the lack of PAR-3::GFP expression in the intestinal and pharynx primordia.

To target the expression of *rab-7* with RNA interference (RNAi) we used feeding protocol 1 described in (Kamath et al., 2001). The effects of *rab-7(RNAi)* were not seen in embryos exposed to *inert/F33E2.4* 9 (RNAi), which targets a gene not involved in gut granule biogenesis or

positioning. Ahringer library clones were used for RNAi (Source Bioscience, Nottingham, UK). In RNAi experiments, inhibition of *rab-7* function was assessed by the appearance of numerous refractile bodies in embryos visualized with DIC microscopy.

2.3. Microscopy

All of the fixed and stained embryos were imaged with a Zeiss LSM710 confocal microscope using a $63\times$ Plan-Apochromat 1.4 NA objective. Living embryos were imaged with a $100\times$ Plan-Acrochromat 100X 1.4 NA objective using a Zeiss AxioImager.M2 widefield

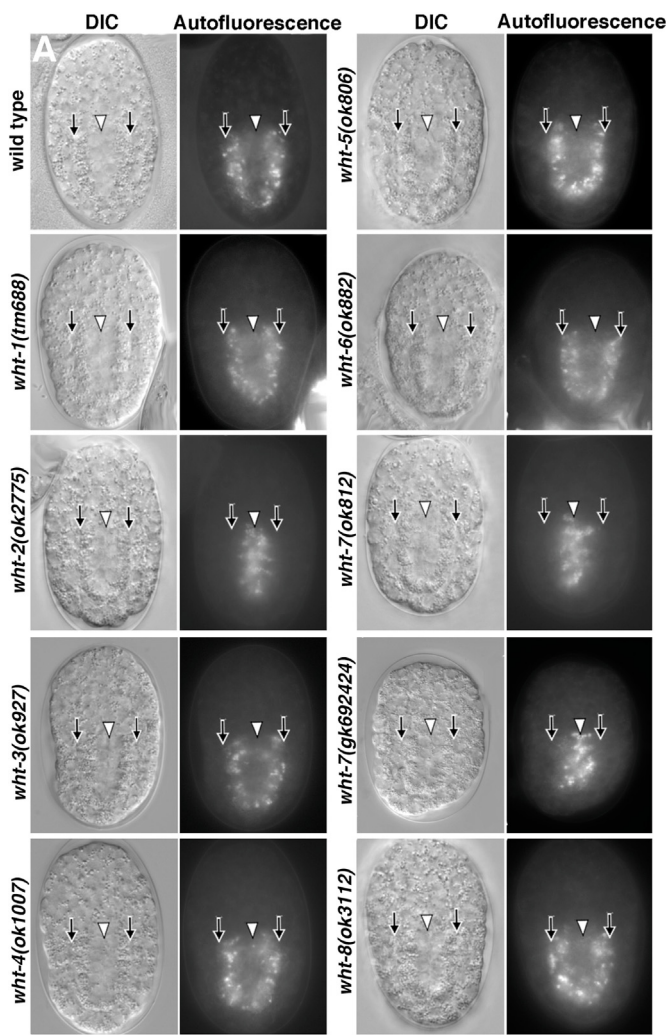


Fig. 8. Screen of WHT family ABCG family proteins for gut granule positioning defects. (A) E16 stage embryos were imaged with DIC and a DAPI fluorescence filter using wide field microscopy to identify the intestinal primordium and autofluorescent gut granules, respectively. The basal surfaces of intestinal cells are marked with black arrows and the apical surfaces are marked with white arrowheads. The DIC and DAPI images show the same optical section. (B) The pattern of gut granule positioning was quantified by categorizing the overall distribution of autofluorescent organelles within the intestinal primordium. The progeny of adults with a PCR product containing *wht-2(+)* or a fosmid containing *wht-7(+)* were scored. Extra-chromosomal arrays are lost during both meiotic and mitotic divisions so that many of the embryos scored lacked the PCR product or fosmid. A Fisher's exact test was used to compare *wht* mutant populations with the extrachromosomal array to the *wht* mutant alone (** represents $p \leq 0.005$).

microscope equipped with DIC, polarization, and fluorescence optics. Images were captured using an AxioCam MRm digital camera controlled by AxioVision 4.8 software (Zeiss, Thornwood, NY).

Living embryos were placed on a 3% agarose pad in a drop of H₂O. Polarization optics were used to visualize birefringent material in 1.5-fold and pretzel stage embryos. Autofluorescence was imaged in E16 stage embryos using a Zeiss 49 filter (DAPI, excitation G 365, emission, BP445/50). Embryos were freeze-cracked and fixed in -20 °C methanol for 15 min (Leung et al., 1999). In some cases the intrinsic fluorescence of GFP was used to visualize GFP tagged proteins. Antibodies to BGS-1 (Moorthy et al., 2000), GFP, including clones 7.1/13.1 (Sigma Aldrich) and ab6556 (abcam), IFA, which binds to centrioles and labels centrosomes (Leung et al., 1999), LMP-1, which labels lysosomes and gut granules (Hadwiger et al., 2010), clone F-11, which binds ICL-1 labeling mitochondria (Liu et al., 1995), clone P4A1, which labels PAR-3 (Nance et al., 2003), PGP-2, which labels gut granules (Schroeder et al., 2007), RAB-5, which labels early endosomes (Audhya et al., 2007), RAB-7, which labels late endosomes (Chen et al., 2010), and WHT-2, which labels gut granules (Voss et al., 2020), were used. We also used two previously undescribed mouse monoclonal antibodies that were identified in a screen for antibodies that label *C. elegans* embryos (Eisenhut et al., 2005). F2-P1C5-A5/Lateral binds only to the lateral domain of polarized epithelial cells in the intestine, pharynx, and hypodermis of *C. elegans* embryos. F2-P3E3-C3/Yolk binds to the exterior of yolk platelets in *C. elegans* embryos. The final antibody washes typically included 0.1 µg/ml DAPI to stain nuclei. Z-stacks spanning the intestine of fluorescently labeled embryos were acquired with confocal microscopy.

Organelle positioning was scored in mid to late E16 stage embryos, which were defined by the developmental stage of the dorsal hypodermis. The mid E16 stage begins when hypodermal cells first extend processes to the opposing end of the contralateral cells. The late E16 stage was defined as the stage when the dorsal hypodermis was fully intercalated prior to elongation of the embryo (Fridolfsson et al., 2018). To enable the best resolution along the apical-basal axis, only embryos that were oriented dorsal or ventral side-up were scored. Z-stacks of antibody stained embryos were analyzed for the focal plane that included the most nuclei from the dorsal tier of E16 stage intestinal cells (Leung et al., 1999). In this optical section, the apical and basal surface of each intestinal cell (typically 10–12 were visible on the chosen focal plane) were identified by labeling the intestinal cell cortex with BGS-1 or the lateral membrane with the Lateral mAb. Occasionally, DAPI stained nuclei were used to define the apical domain as the region between contralateral intestinal nuclei and the basal domain as the surface of the underlying muscle cell nuclei. The apical to basal axis was then divided into 4 equal quadrants using a clear acetate sheet placed over the image projected on a computer monitor. The number of organelles present in each quadrant was then quantified for each intestinal cell per embryo in at least 5 different embryos. To present the data graphically, the square root of the total proportion of organelles located in each quadrant was calculated and used as the radius of the circles drawn to represent each proportion using R (version 3.1.2). Therefore, the area of each circle is directly proportional to the percentage of compartments found in that quadrant. Widefield fluorescence microscopy was used to score gut granule positioning in living embryos. After determining the correct stage and orientation with DIC microscopy, the focal plane that included the most nuclei from the dorsal tier of E16 stage intestinal cells was chosen. At this focal plane the overall pattern of autofluorescent organelles was then scored.

The SQUASH module within FIJI was used to quantify the colocalization of fluorescent markers (Rizk et al., 2014; Schindelin et al., 2012). This software segments and identifies labeled organelles within Z-stacks spanning the intestine and calculates the fraction of the volume of one marker that overlaps with the second marker.

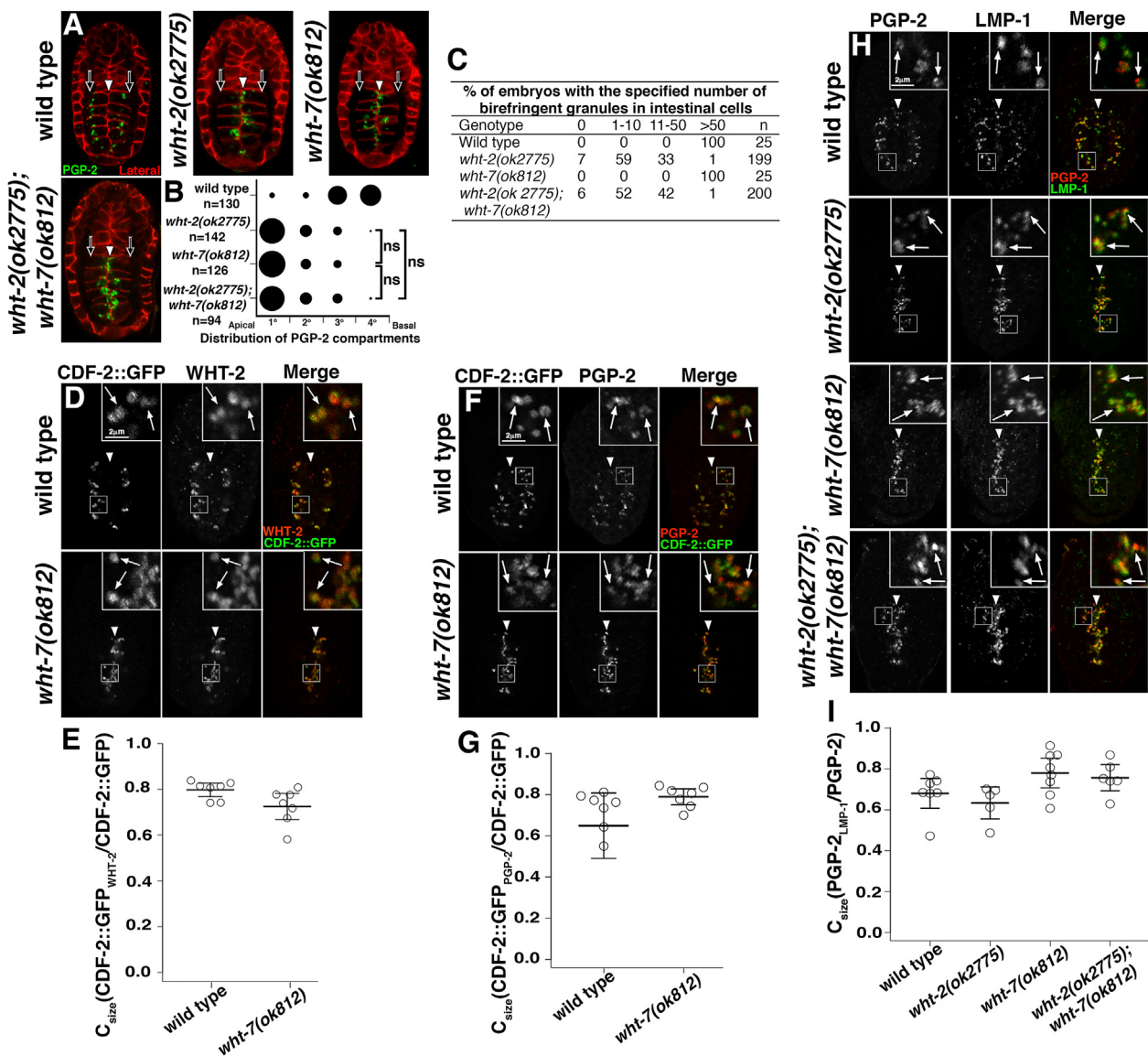


Fig. 9. Effects of *wht-7*(*-*) on gut granule positioning and gut granule formation. (A) E16 stage embryos were stained with antibodies marking PGP-2 and lateral domains and imaged with confocal microscopy. Single optical sections are shown, and white arrowheads and black arrows mark the apical and basal intestinal cell domains, respectively. (B) The position of organelles within individual intestinal cells was scored as described in the legend for Fig. 1. The size of the circles represents the proportion of organelles located within each quadrant. A Fisher's exact test was used to compare the distribution of PGP-2 marked organelles between the single and double mutants as indicated by the brackets (ns represents a $p > 0.05$). (C) Three-fold and later stage embryos were analyzed using polarization microscopy and scored for the number of birefringent granules in the intestine. The *wht-2;wht-7* double mutant was not significantly different than *wht-2* (*ok2775*) ($p > 0.05$, Fisher's exact test). (D, F, H) The relative localization of gut granule proteins CDF-2::GFP, WHT-2, PGP-2, and LMP-1 was assessed in E16 stage embryos with confocal microscopy. In insets, white arrows denote compartments containing both markers. (E, G, I) SQUAASH software was used to calculate C_{size} , which describes the proportion of the total CDF-2::GFP or PGP-2 area within an embryo that also contains the indicated marker. Five to seven embryos were analyzed. The mean is plotted and the error bars represent the 95% confidence limit. Wild type and mutants were compared to each other with a one-way ANOVA and $p > 0.05$.

One-way ANOVAs and Tukey-Kramer post hoc tests were carried out with Microsoft Excel for Mac 2011. Fisher's exact tests were carried out at www.physics.csbsju.edu/stats/exact_NROW_NCOLUMN_form.html. Dot plots were created with R. Photoshop CS2 was used to construct figures and adjustments in brightness and contrast were uniformly applied to each panel. Representative images of organelle position and marker colocalization are shown.

3. Data availability

Strains and antibodies are available upon request. All of the data necessary for judging the conclusions of the article are present with the figures and graphs.

4. Results

4.1. Asymmetric localization of organelles during epithelial polarization

Intestinal organogenesis initiates through the rapid divisions of the intestinal precursor E and its descendants, which clonally produce the twenty cells that compose the intestine (Sulston, 1976). The number of E descendants present within the intestinal primordium is commonly used to describe the different stages of intestinal development. Following the E8 to E16 cell divisions, E16 intestinal cells rapidly establish cell-cell junctions and cortically polarize so that their apical surface faces the intestinal lumen located at the midline between the cells on left and right sides of the bilaterally symmetric intestine (Leung et al., 1999). The

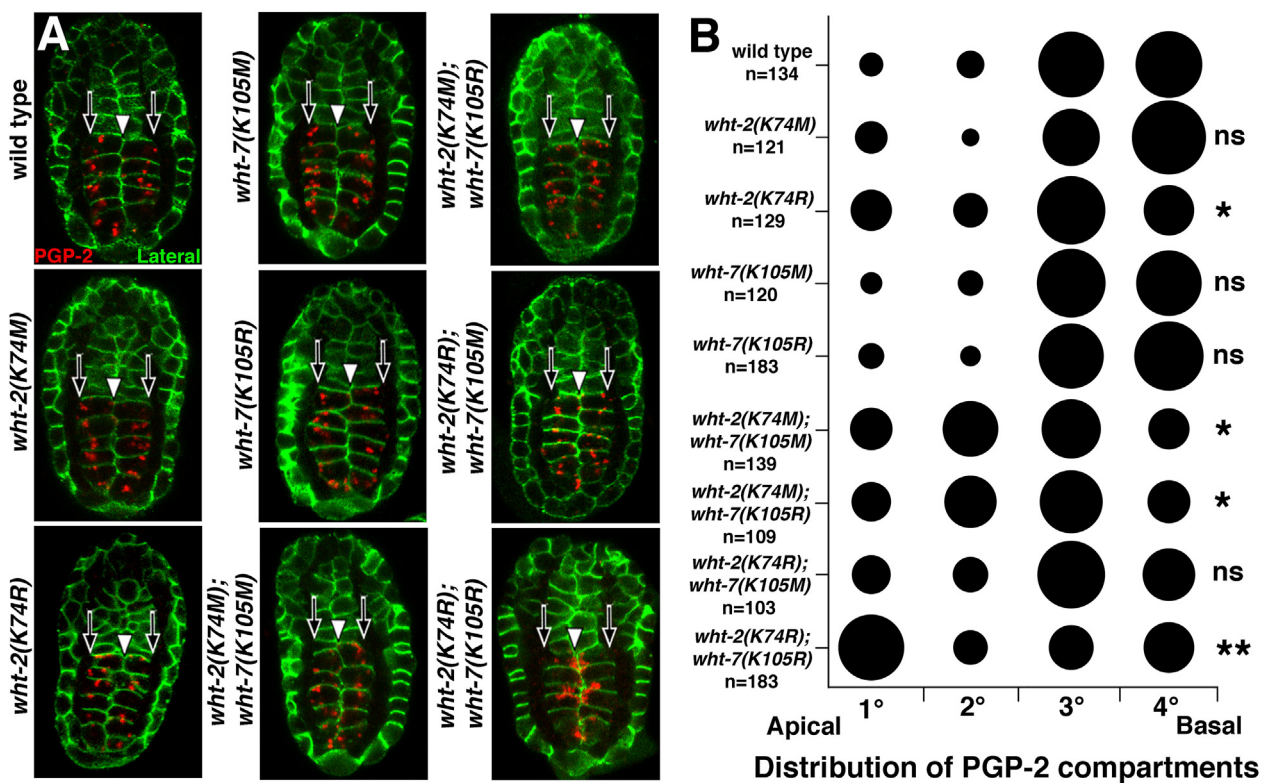


Fig. 10. Gut granule positioning in WHT-2 and WHT-7 ATPase mutants. (A) E16 stage embryos were stained with antibodies marking PGP-2 and lateral domains and imaged with confocal microscopy. Single optical sections are shown, and white arrowheads and black arrows mark the apical and basal intestinal cell domains, respectively. (B) The position of organelles within individual intestinal cells was scored as described in the legend for Fig. 1. The size of the circles represents the proportion of organelles located within each quadrant. A Fisher's exact test followed by a Bonferroni correction was used to compare the distribution of PGP-2 compartment positioning in the single mutants and wild type or the double mutants and the single mutants used to construct it (ns is $p > 0.05$, * is $p \leq 0.05$, ** is $p \leq 0.001$).

opposing basal surfaces face surrounding muscle and epidermal cells (Leung et al., 1999). At the same time, nuclei and their associated centrosomes become asymmetrically positioned near the apical membrane (Starr et al., 2001) (Fig. 1A and B), indicating that the cytoplasm also becomes polarized at this stage of intestinal development.

To investigate whether other organelles become asymmetrically positioned in intestinal cells at the time that they establish cortical polarity, we surveyed the subcellular distribution of organelles using well-characterized organelle markers in fixed E16 stage intestinal cells. The apical and basal surfaces were identified by staining with antibodies to the β -spectrin cell cortex protein (BGS-1), by staining with a monoclonal antibody that recognizes an unidentified epitope in the lateral domain of epithelial cells (Lateral), or by labeling nuclei to aid in inferring the position of the intestinal cell cortex. We scored organelle position by subdividing intestinal cells into four equally sized quadrants along the apico-basal axis and quantified the number of organelles within each quadrant. For nuclei, which are larger than a single quadrant, we divided the apico-basal axis into thirds. The results are represented by circles that are directly proportional to the percentage of an organelle found within each quadrant (Fig. 1B). Notably, most of the organelles we examined exhibited some level of asymmetry. All of the conventional endosomal organelles, including early endosomes, late endosomes, and lysosomes, were highly enriched near the apical cell membrane (Fig. 1A and B). We confirmed prior work suggested that gut granules, lysosome-related organelles that are part of the endosomal system, are positioned basally (Fig. 1A and B) (Leung et al., 1999; Hermann et al., 2005, 2012; Davis et al., 2009). Yolk platelets, lipid droplets, and to a lesser extent mitochondria, were also basally localized (Fig. 1A and B). The Golgi exhibited little if any polarization along the apico-basal axis (Fig. 1A and B).

To determine when these organelles become asymmetrically positioned, we analyzed their distribution along the midline to basal cell axis in the E8 stage intestinal primordium. None of the organelles we examined in E8 stage intestinal cells, including nuclei, conventional endosomes, gut granules, yolk platelets, and lipid droplets, exhibited the level of polarization seen in E16 cells, often being distributed uniformly throughout the cytoplasm (Fig. 2A and B). Therefore, during the E16 stage the intestinal cell cytoplasm undergoes a dramatic reorganization and polarization at the same time that intestinal cells establish cortical asymmetry along the apical-basal axis.

4.2. Nuclear polarization promotes the basal positioning of some organelles

We addressed the possibility that the localization of nuclei, which take up a significant fraction of the apical cell domain (Fig. 1A), contribute to the organelle asymmetries exhibited by E16 stage intestinal cells. For example, organelles might be displaced basally in response to apical nuclear positioning or, alternatively, organelles might associate with nuclei to become apically polarized. Nuclear migration from a central position in E8 cells to the apical domain in E16 intestinal requires UNC-83 (Starr et al., 2001), which is part of the evolutionarily conserved LINC complex that mediates nuclear movements (Bone and Starr, 2016). As expected for an organelle closely associated with the nucleus (Burakov and Nadezhina, 2013), centrosomes became displaced from the apical surface in *unc-83(ku18)* mutants that have centrally positioned nuclei (Fig. 1A and B). The distribution of early endosomes, late endosomes, and lysosomes remained apical in *unc-83(–)*, showing that their asymmetric localization is independent of nuclear migration. In contrast, most of the basally polarized organelles, including gut granules and yolk platelets,

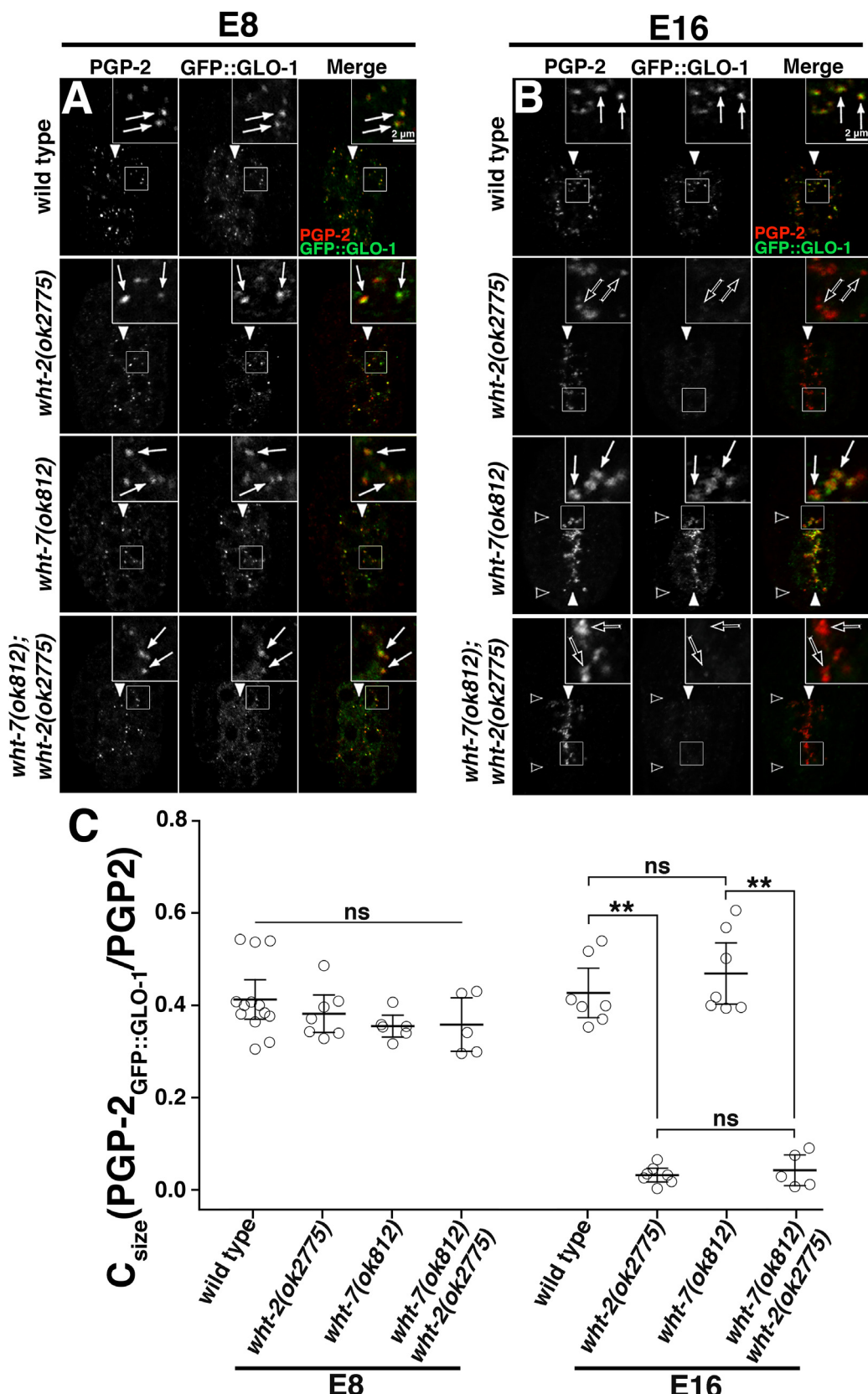


Fig. 11. Effects of *wht-2(–)* and *wht-7(–)* on GFP::GLO-1 localization in E8 and E16 stage embryos. (A) E16 stage embryos expressing GFP::GLO-1 were stained with antibodies to PGP-2 and GFP and imaged with confocal microscopy. White arrows indicate examples of GFP::GLO-1 localizing to PGP-2 compartments and black arrows indicate examples where GFP::GLO-1 is lacking from PGP-2 compartments. (B) The proportion of the total PGP-2 signal area in each embryo that also contains GFP::GLO-1 is plotted. Five to 13 embryos of each genotype were analyzed. The mean is shown and the bars represent the 95% confidence interval. Strains were compared to each other by one-way ANOVA (ns is $p > 0.05$ and ** is $p \leq 0.001$).

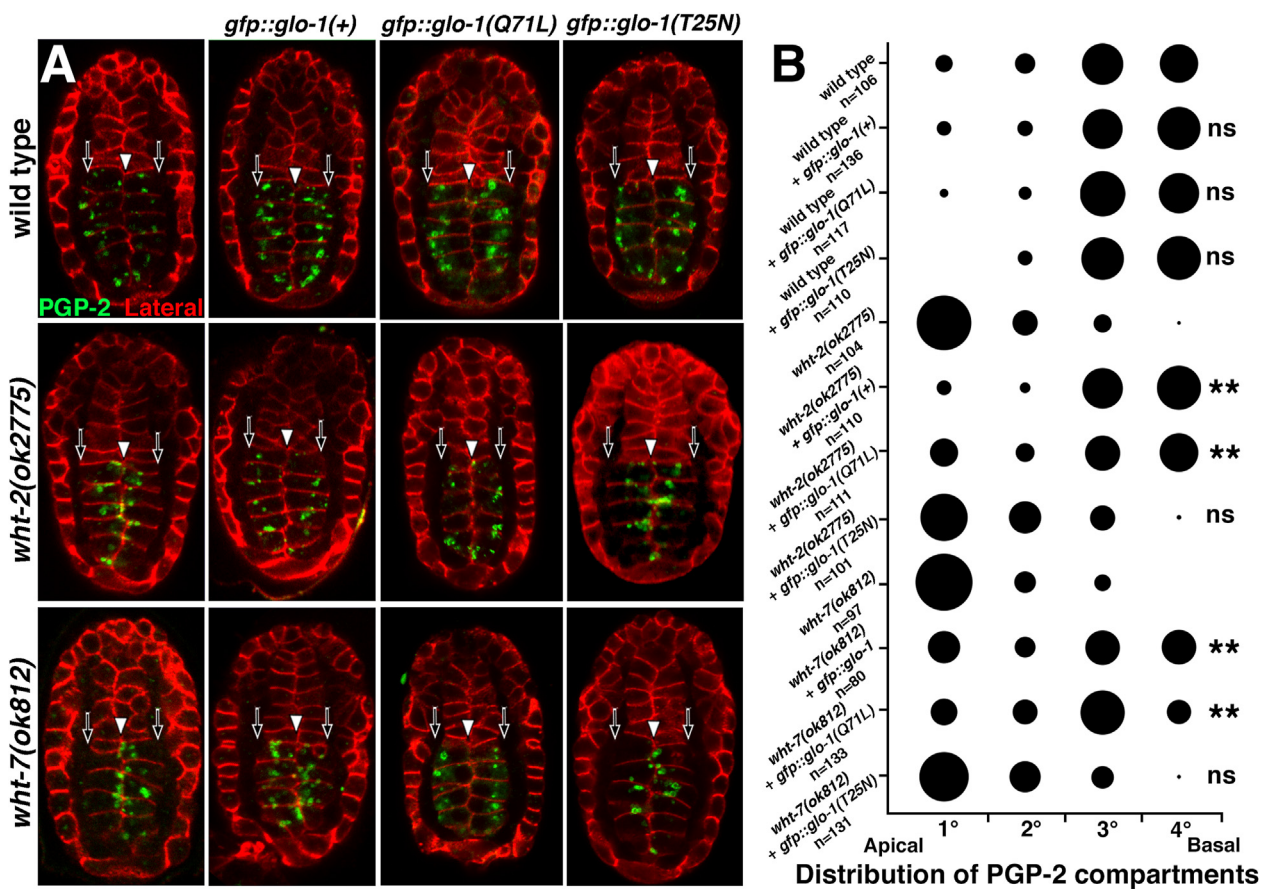


Fig. 12. Expression of GLO-1 restores basal gut granule positioning in *wht-2*(–) and *wht-7*(–) mutants. (A) E16 stage embryos lacking or expressing different forms of GFP:GLO-1 were stained with antibodies marking PGP-2 and lateral domains and imaged with confocal microscopy. Single optical sections are shown, and white arrowheads and black arrows mark the apical and basal intestinal cell domains, respectively. (B) The position of organelles within individual intestinal cells was scored as described in the legend for Fig. 1. The size of the circles represents the proportion of organelles located within each quadrant. A Fisher's exact test followed by a Bonferroni correction was used to compare the distribution of PGP-2 compartment positioning in embryos expressing *gfp::glo-1* to those lacking its expression (ns is $p > 0.05$ and ** is $p \leq 0.001$).

became uniformly distributed along the apical-basal axis when nuclear migration was disrupted (Fig. 1A and B). Therefore, the basal polarization of some organelles might be due to their exclusion from the apical domain by the nucleus. The exceptions to this were lipid droplets, which remained basally polarized in *unc-83*(–) mutants (Fig. 1A and B).

4.3. PAR-3 is dispensable for organelle asymmetry in intestinal epithelial cells

The PAR polarity proteins are central regulators of cell cortex asymmetry (Lang and Munro, 2017). Notably, the PAR system mediates the asymmetric positioning of nuclear DNA and early endosomes in the one-cell *C. elegans* embryo and endosomes in adult *C. elegans* intestinal cells (Winter et al., 2012; Andrews and Ahringer, 2007; Kemphues et al., 1988). Given the requirement for PAR-3 in these processes, we investigated whether PAR-3 functioned in the polarized distribution of organelles in the E16 stage intestinal primordium. We analyzed organelle positioning in *par-3*(–) embryos in which maternally supplied PAR-3 was depleted using the *par-3*(MZ) targeted protein degradation system, which has been shown to potently remove PAR-3 in E16 stage intestinal cells (Achilleos et al., 2010). Early endosomes, late endosomes, and nuclei continued to be positioned apically and gut granules remained basally positioned in embryos lacking PAR-3 (Fig. 3A and B), indicating that cytoplasmic polarization is independent of the PAR polarity pathway.

4.4. *wht-2*(–) mutants mislocalize gut granules apically

In a screen of the *C. elegans* Million Mutation collection for strains exhibiting altered LRO number or size, we identified one strain, VC40939, which mispositioned autofluorescent gut granules apically in E16 stage embryos. Each of the Million Mutation strains has had its genome sequenced and VC40939 contains *wht-2(gk891224)*, a non-sense mutation (Q49stop) that likely disrupts the function of WHT-2 (Thompson et al., 2013). *wht-2* encodes an ABCG protein homologous to *Drosophila* White and mammalian ABCG proteins that promote multidrug resistance (Sarkadi et al., 2006; Sheps et al., 2004). We have recently shown that WHT-2 plays a role in gut granule biogenesis and localizes to E20 stage gut granules (Voss et al., 2020). We examined WHT-2 localization in earlier embryonic stages and found that it is localized to gut granules prior to and during the stage that they become asymmetrically positioned along the apico-basal axis (Fig. S1). Embryos with the *wht-2(ok2775)* null mutation showed apical gut granule mispositioning similar to *wht-2(gk891224)*, which was rescued by the addition of *wht-2*(+) (Fig. 4A and B). Together these results indicate that WHT-2 functions to prevent the apical localization of gut granules.

Gut granules were often closely associated with apically localized nuclei in *wht-2*(–) mutants (Fig. 4A). To determine whether gut granules become mispositioned in *wht-2*(–) mutants due to an inappropriate interaction with nuclei, we analyzed gut granule localization when nuclei

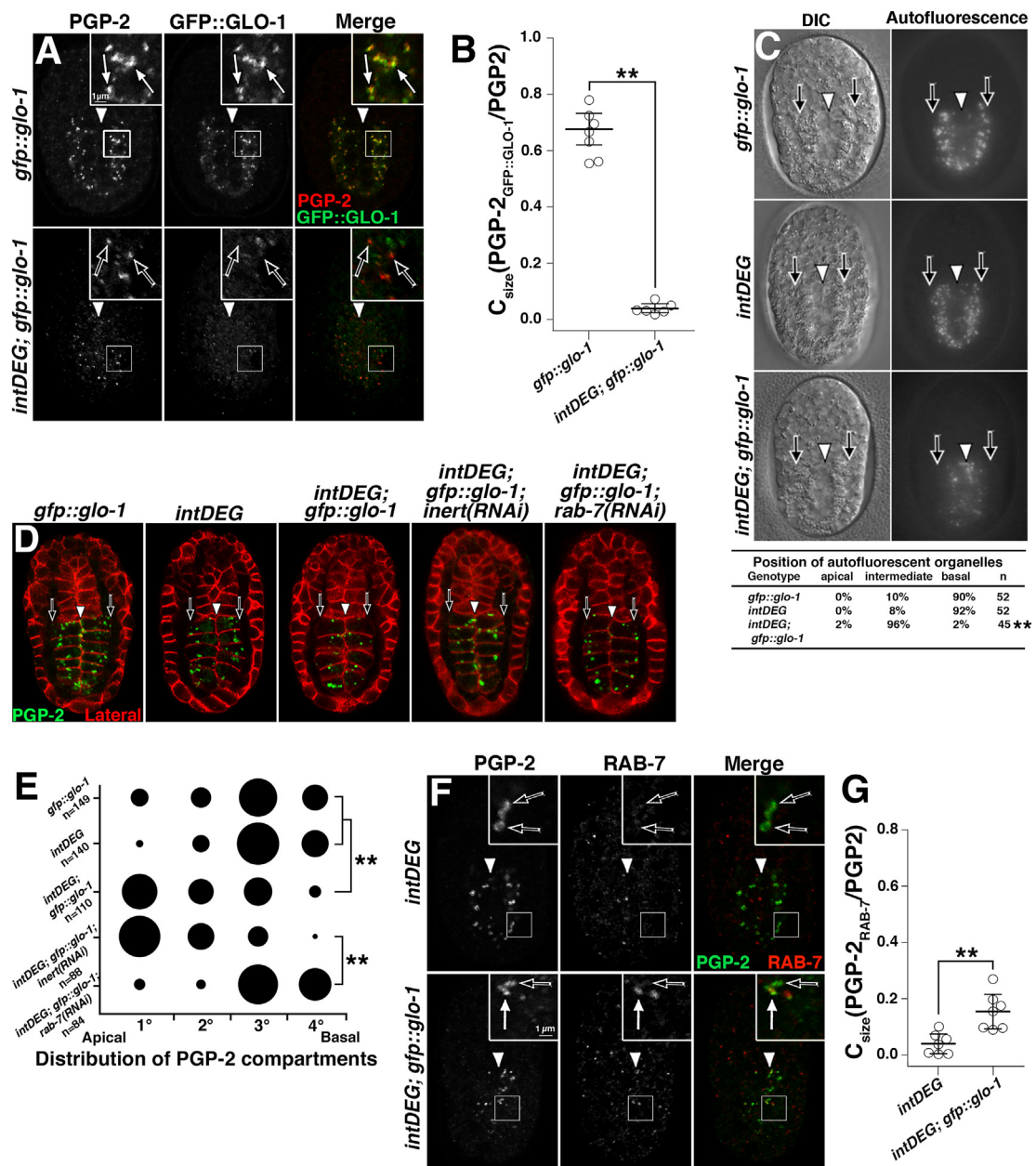


Fig. 13. Role of GLO-1 in gut granule positioning during epithelial polarization. (A) E16 stage embryos expressing *gfp::glo-1* were stained with antibodies to PGP-2 and GFP and imaged with confocal microscopy. White arrows indicate examples of GFP::GLO-1 localizing to PGP-2 compartments and black arrows indicate examples where GFP::GLO-1 is lacking from PGP-2 compartments. (B) The proportion of the total PGP-2 signal area in each embryo that also contained GFP::GLO-1 is plotted. The mean is shown and the bars represent the 95% confidence interval. Strains were compared to each other by one-way ANOVA (** is $p \leq 0.001$). (C) E16 stage embryos were imaged with DIC and a DAPI fluorescence filter using wide field microscopy and the overall distribution of autofluorescent organelles within the intestinal primordium was categorizing. The basal surfaces of intestinal cells are marked with black arrows and the apical surfaces are marked with white arrowheads. The DIC and DAPI images show the same optical section. A Fisher's exact test was used to compare *intDEG; gfp::glo-1* with the *intDEG* and *gfp::glo-1* populations (** represents $p \leq 0.005$). (D) E16 stage embryos were stained with antibodies marking PGP-2 and lateral domains and imaged with confocal microscopy. Single optical sections are shown, and white arrowheads and black arrows mark the apical and basal intestinal cell domains, respectively. (E) The position of organelles within individual intestinal cells was scored as described in the legend for Fig. 1. In E, the size of the circles represents the proportion of organelles located within each quadrant. A Fisher's exact test was used to compare the distribution of PGP-2 compartment positioning in the indicated strains (** is $p \leq 0.001$). (F) E16 stage embryos were stained with antibodies to PGP-2 and RAB-7 and imaged with confocal microscopy. White arrows indicate examples of RAB-7 localizing to PGP-2 compartments and black arrows indicate examples where GFP::GLO-1 is lacking from PGP-2 compartments. (G) The proportion of the total PGP-2 signal area in each embryo that also contained RAB-7 is plotted. The mean is shown and the bars represent the 95% confidence interval. Strains were compared to each other by one-way ANOVA (** is $p \leq 0.001$).

were centrally positioned in *unc-83*(-). We found that the apical localization of gut granules in *wht-2*(-) remained unchanged by the loss of *unc-83*(+) (Fig. 4A and B), indicating that other processes are directing their apical accumulation.

We investigated whether the mislocalization of gut granules in *wht-2*(-) mutants results from larger changes in the apico-basal cytoplasmic polarity of E16 stage intestinal cells. As in wild type, early endosomes, late endosomes, lysosomes, nuclei, and centrosomes were apically

localized in *wht-2(–)* mutants (Fig. 5A and B). Similarly, the positioning of basally enriched organelles including yolk platelets, mitochondria, and lipid droplets were unchanged in *wht-2(–)* mutants (Fig. 5A and B). These results show that cytoplasmic polarity is normal when WHT-2 function is disrupted and that the effects of *wht-2(–)* are specific to gut granule positioning.

4.5. Apical gut granules in *wht-2(–)* mutants do not resemble endolysosomes

CDF-2::GFP, which associates with gut granules in wild type (Davis et al., 2009; Hermann et al., 2012), marks apically positioned organelles in *wht-2(–)* mutants (Fig. 4A and B). We found that two gut granule membrane proteins, PGP-2 and LMP-1 (Schroeder et al., 2007; Hermann et al., 2012), co-localized with CDF-2::GFP in E16 stage *wht-2(–)* embryos, just as they did in wild type (Fig. 6A and B), making it unlikely that CDF-2::GFP is lacking from gut granules and mislocalized to apical organelles in *wht-2(–)*. In addition, *wht-2(–)* did not cause CDF-2::GFP or PGP-2 to colocalize with the lysosomal proteins ASM-1::mCherry or LAAT-1::GFP (Levitte et al., 2010; Liu et al., 2012) (Fig. 6A–C), which are localized to apically positioned conventional endosomes in E16 intestinal cells (Fig. 1A and B). We therefore conclude that bona fide gut granules, which are distinct from conventional lysosomes, are being apically mispositioned in *wht-2(–)* (Fig. 6A and B).

LROs are part of the endolysosomal system, sharing similarities with and utilizing many of the same factors that mediate the movement of proteins between conventional endosomes (Bowman et al., 2019). We therefore addressed the possibility that gut granules in *wht-2(–)* E16 stage intestinal cells take on a conventional endosomal identity or misaccumulate endosomal positioning factors. The small GTPases RAB-5, RAB-7, and ARL-8::GFP are enriched on and can direct the movement of early endosomes, late endosomes, and lysosomes, respectively (Sato et al., 2014). RAB-7 and ARL-8::GFP were not detectable on gut granules in wild type or *wht-2(–)* (Fig. 6A–C). While we observed a slight increase in the colocalization of RAB-5 with CDF-2::GFP, *wht-2(–)* did not lead to the accumulation of early endosomal phosphatidylinositol 3-phosphate, which is bound by FYVE::GFP (Dumas et al., 2001), on PGP-2 labeled gut granules (Fig. 6A–C). Together, these results indicate that conventional endosomes and gut granules remain distinct when *wht-2(+)* activity is disrupted and that factors directing conventional endosome motility are not obviously mislocalized to gut granules in *wht-2(–)* mutants.

4.6. Defects in gut granule biogenesis disrupt gut granule positioning differently than *wht-2(–)*

The specific and acute mislocalization of gut granules in *wht-2(–)* suggests that in wild type, gut granules are actively prevented from localizing apically. To further explore the mechanisms governing gut granule positioning, we investigated whether gut granule identity is necessary for their basal positioning. *apt-6*, *glo-2*, *glo-3*, *rab-7*, and *yps-18* mutants disrupt protein delivery pathways leading to gut granules and have altered gut granules marked by PGP-2 (Morris et al., 2018; Hermann et al., 2012; Delahaye et al., 2014). We found that the absence of RAB-7 or the AP-3 complex subunit APT-6 had little effect on the basal positioning of gut granules (Fig. 7A and B). In contrast, there was a significant increase in the proportion of gut granules localized apically when the function of the BLOC-1 subunit GLO-2, the HOPS subunit VPS-18, or the likely Rab guanine exchange factor subunit GLO-3 were disrupted (Fig. 7A and B). *glo-2(tm592)* is cold sensitive for defects in gut granule biogenesis (Hermann et al., 2012), and consistent with this causing gut granule mispositioning, the proportion of apical gut granules was enhanced at 15C (Fig. 7A and B). Nuclei were always positioned apically in the gut granule biogenesis mutants ($n = 5–26$ embryos per strain).

While mutants disrupting gut granule biogenesis sometimes altered gut granule positioning, none of them led to the high levels of apical gut

granule enrichment seen in *wht-2(–)* mutants. To explore whether WHT-2 promotes gut granule positioning through a role in gut granule biogenesis or through a different mechanism, we combined *wht-2(–)* with *glo-3(kx38)* and *rab-7(RNAi)*, both of which disrupt protein trafficking to gut granules (Morris et al., 2018; Delahaye et al., 2014). The addition of *glo-3(kx38)* disrupted the apical localization of gut granules caused by *wht-2(–)* and *wht-2(ok2775)*; *glo-3(kx38)* double mutants closely resembled the *glo-3(kx38)* single mutant, where the majority of gut granules are located in basal quadrants (Fig. 7A and B). *rab-7(RNAi)* similarly caused most gut granules to become basally positioned in *wht-2(–)* (Fig. 7A and B). The effects of *glo-3(kx38)* and *rab-7(RNAi)* on the localization of gut granules in *wht-2(–)* suggests that gut granule identity is necessary for their apical mispositioning and that general defects in gut granule protein trafficking are unlikely to underlie the mislocalization of gut granules in *wht-2(–)*.

4.7. The ABCG protein WHT-7 functions in gut granule positioning

WHT-2 is one of eight WHT/ABCG family members in *C. elegans* (Sheps et al., 2004). ABCG proteins are often described as half transporters, due to the requirement that they homo- or heterodimerize with another ABCG protein to constitute a functional transporter (Tarr et al., 2009). To investigate whether WHT-2 functions with another ABCG protein, we analyzed autofluorescent gut granule positioning in E16 stage intestinal cells in embryos containing mutations that disrupt the function of each of the seven other *wht* genes. We found that strains containing the deletion allele *ok812* or the *gk692424* nonsense mutation, both of which are predicted to be null for *wht-7* activity, showed apical enrichment of autofluorescent organelles (Fig. 8A and B). None of the other *wht* gene mutants disrupted gut granule positioning (Fig. 8A and B). Introduction of a fosmid containing *wht-7(+)* into the *wht-7(ok812)* mutant restored the basal positioning of PGP-2 marked compartments (Fig. 8B). The apical organelles in *wht-7(–)* appear to be properly formed gut granules based on the high level of colocalization between PGP-2 and both CDF-2::GFP and LMP-1 (Fig. 9F–I). These results indicate that *wht-7(–)*, like *wht-2(–)*, causes the apical enrichment of gut granules in E16 intestinal cells.

Since both *wht-2* and *wht-7* encode ABCG proteins that could work together, we investigated the functional relationship between WHT-2 and WHT-7. Consistent with WHT-2 and WHT-7 acting in the same process, gut granule positioning in E16 intestinal cells was indistinguishable between *wht-2(–)*, *wht-7(–)*, and *wht-2(–); wht-7(–)* double mutants (Fig. 9A and B). Additionally, *rab-7(RNAi)* suppressed apical gut granule mispositioning in *wht-7(–)* mutants, similar to its suppression of *wht-2(–)* (Fig. 7A and B). WHT-2 remained associated with gut granules in the *wht-7(–)* mutant at the time when gut granules polarize in E16 intestinal cells (Fig. 9D and E), indicating that WHT-7 does not direct the localization of WHT-2.

In addition to functioning in gut granule positioning, WHT-2 plays a role in gut granule biogenesis (Voss et al., 2020). However, unlike *wht-2(–)*, the accumulation of birefringent material within gut granules was unchanged in *wht-7(–)* and the number of birefringent gut granules in *wht-2(–)*; *wht-7(–)* double mutants resembled the *wht-2(–)* single mutant (Fig. 9C). *wht-2(–)* suppresses gut granule enlargement and enhances the loss of LMP-1 from gut granules in *glo-3(–)* mutants (Voss et al., 2020). *wht-7(–)* mutants did not alter either of these *glo-3(–)* phenotypes (Fig. S2). Additionally, *wht-2(–); wht-7(–)* double mutants did not show any reduction in the colocalization of the gut granule proteins PGP-2 and LMP-1 (Fig. 9H and I). These data are consistent with WHT-2 and WHT-7 functioning similarly in gut granule positioning and highlight their different requirements for supporting gut granule biogenesis. Furthermore, they suggest that the mislocalization of gut granules in *wht-2(–)* and *wht-7(–)* is not the result of defective gut granule biogenesis.

4.8. WHT-2 and WHT-7 ATPase activity promotes gut granule positioning

The similar effects of *wht-2(–)* and *wht-7(–)* on gut granule distribution suggest that WHT-2 and WHT-7 proteins might associate and function together as a membrane transporter. We analyzed gut granule positioning in WHT-2 and WHT-7 point mutants predicted to inhibit their ATPase activity, which is essential for ABCG proteins to translocate substrates across membranes (Taylor et al., 2017). Changing the conserved lysine in the Walker A motif to a methionine or arginine disrupts both the ATPase and transporter activity of ABCG proteins (Henriksen et al., 2005; Ozvegy et al., 2002; Zhang et al., 2006). We have previously shown that the WHT-2(K74M) and WHT-2(K74R) point mutants partially disrupt the function of WHT-2 in gut granule biogenesis (Voss et al., 2020). We used CRISPR/Cas9 genome editing to precisely alter the endogenous *wht-7* locus and generated WHT-7(K105M) and WHT-7(K105R) Walker A motif point mutants. The WHT-2(K74M) and both WHT-7 ATPase mutants did not disrupt gut granule positioning (Fig. 10A and B). Only WHT-2(K74R) showed a discernible increase in the proportion of gut granules located in the apical domain (Fig. 10A and B), but the effect was quite weak when compared to the *wht-2(–)* null mutant (Fig. 4A and B).

ABCG transporters create two ATP binding sites using structural components from each of the opposing subunits (Eckenstaler and Bendorf, 2020). If WHT-2 and WHT-7 function as homodimers, then the single ATPase mutants should disrupt their ATPase and coupled membrane transport activity. However, ABCG proteins can form heterodimers (Hegyi and Homolya, 2016; Cserepes et al., 2004). If WHT-2 and WHT-7 heterodimerize, then a single functional ATPase domain would remain when a single WHT-2 or WHT-7 Walker A mutant is expressed, which can be sufficient for ABC transporter function (Zhang et al., 2006; Gao et al., 2000; Perria et al., 2006; Procko et al., 2006). We therefore analyzed gut granule positioning in WHT-2 and WHT-7 ATPase double mutants and found an apical enrichment of gut granules in WHT-2(K74R); WHT-7(K105R) double mutants that approached the effect seen in *wht-2(–)* and *wht-7(–)* null mutants (Figs. 4A and B, 9A–B, and 10A–B). Combining WHT-2(K74M) with either WHT-7 ATPase mutant led to a modest defect in gut granule polarization that was not seen in the single mutants (Fig. 10A and B). These synergistic and synthetic genetic interactions between WHT-2 and WHT-7 ATPase mutants suggest that a WHT-2/WHT-7 heterodimer functions as a membrane transporter to promote gut granule positioning. However, none of the single or double ATPase mutants led to the strong apical enrichment seen in *wht-2(–)* or *wht-7(–)*, which could be explained by ATPase independent activity or homodimerization of WHT-2 and WHT-7 promoting basal gut granule localization.

4.9. Effects of *wht-2(–)* and *wht-7(–)* on GLO-1 Rab localization

Small GTPases, including Rabs and Arfs, localize to endosomes and mediate their intracellular localization (Ballabio and Bonifacino, 2020; Neefjes et al., 2017). WHT-2 is necessary for the association of the Rab32/38 family member GLO-1 with E20 stage gut granules (Voss et al., 2020), an embryonic stage after gut granules become asymmetrically localized. We examined GFP::GLO-1 localization in earlier E8 and E16 stage embryos and found that GLO-1 was associated with gut granules where it could function to position gut granules in polarizing intestinal cells (Fig. 11A–C). In *wht-2(–)* mutants, GFP::GLO-1 was enriched on E8 stage gut granules, but GFP::GLO-1 was lacking from gut granules in E16 stage intestinal cells (Fig. 11A–C).

Given the possibility that WHT-7 functions with WHT-2 to promote gut granule positioning, we investigated the localization of GFP::GLO-1 in embryos lacking *wht-7* activity. Similar to *wht-2(–)* mutants, gut granules in E8 stage *wht-7(–)* mutants were marked by GFP::GLO-1 (Fig. 11A and C). However, GFP::GLO-1 remained associated with gut granules in E16 stage *wht-7(–)* mutants (Fig. 11B and C), which was surprising given evidence for the WHT-2/WHT-7 heterodimer (Fig. 10).

wht-2(–); wht-7(–) double mutants retained GFP::GLO-1 on gut granules at the E8 stage and lacked GFP::GLO-1 on gut granules at the E16 stage, similar to *wht-2(–)* single mutants. Therefore, in contrast to WHT-2, WHT-7 is not necessary for the accumulation of GLO-1 on gut granules at the time that they are basally positioned.

4.10. GLO-1 Rab activity impacts gut granule positioning

If the loss of GLO-1 from gut granules in *wht-2(–)* leads to their apical accumulation, then the ectopic overexpression of GFP::GLO-1 might restore their basal localization. We introduced GFP::GLO-1 on an extra-chromosomal array into *wht-2(–)* and found that it potently suppressed gut granule mispositioning (Fig. 12A and B). To determine whether the GTPase activity of GLO-1 was necessary for this effect, we expressed GFP::GLO-1(Q71L) and GFP::GLO-1(T25N), which are predicted to be locked in the GTP and GDP-bound states, respectively. While GLO-1(Q71L) suppressed gut granule mispositioning in *wht-2(–)*, GLO-1(T25N) did not (Fig. 12A and B). The expression of GLO-1(+) and GLO-1(Q71L), but not GLO-1(T25N), similarly promoted the basal localization of gut granules in *wht-7(–)* mutants (Fig. 12A and B). These results are consistent with GLO-1 acting as a GTPase downstream of WHT-2 and WHT-7 to promote proper gut granule distribution.

If GLO-1 directs the basal positioning of gut granules, then disrupting its activity should alter gut granule distribution. However, *glo-1(+)* is necessary for the creation of gut granules (Hermann et al., 2005; Morris et al., 2018). To circumvent this limitation, we targeted GLO-1 for destruction after gut granules have been created with an approach that temporally and spatially controls protein degradation (Wang et al., 2017). In this system the intestine specific *elt-2* promoter drives the expression of a GFP nanobody::ZIF-1 fusion (called intDEG) at the E8 stage leading to potent and selective proteosomal degradation of GFP tagged proteins (Wang et al., 2017). Combining endogenously tagged *gfp::glo-1* with intDEG led to the loss of GFP::GLO-1 from E16 intestinal cells (Fig. 13A and B). In contrast to *glo-1(–)* mutants that lack gut granules (Hermann et al., 2005; Morris et al., 2018), organelles containing gut granule associated PGP-2, autofluorescent material, and WHT-2 were detected in *intDEG; gfp::glo-1* E16 intestinal cells, indicating that gut granules are present (Fig. 13A and C, and S3). In embryos where *gfp::glo-1* was targeted for degradation, autofluorescent gut granules were no longer basally enriched (Fig. 13C). We quantified gut granule localization and found that most were localized apically in the *intDEG; gfp::glo-1* strain (Fig. 13D and E), suggesting that GLO-1 activity mediates the basal localization of gut granules. The normal morphology and distribution of WHT-2 in *intDEG; gfp::glo-1* E16 stage embryos strongly suggests that degradation of GLO-1 does not disrupt the gut granule localization and function of WHT-2 in gut granule positioning (Fig. S3).

Rab7 directs endolysosome motility and GLO-1 activity can repress the association of RAB-7 with gut granules (Ballabio and Bonifacino, 2020; Neefjes et al., 2017; Morris et al., 2018). We found that the localization of RAB-7 to gut granules was slightly elevated in *intDEG; gfp::glo-1* embryos (Fig. 13F and G) and that *rab-7(RNAi)* suppressed the apical mislocalization of gut granules in *intDEG; gfp::glo-1* embryos. These observations are consistent with RAB-7 directing the apical positioning of gut granules when GLO-1 is targeted for degradation (Fig. 13D and E).

5. Discussion

5.1. Organelle positioning during epithelial polarization

Coincident with apico-basal polarization of the cell cortex and the establishment of epithelial cell-cell junctions within the intestinal primordium (Leung et al., 1999), our work shows that *C. elegans* intestinal cells establish dramatic asymmetries in organelle positioning along the apico-basal axis. Along with the nucleus, organelles composing the conventional endolysosomal pathway were localized near the apical cortex (Fig. 1). Conversely, gut granules, yolk platelets, and lipid droplets

were highly enriched basally (Fig. 1). Mitochondria, while basally biased, were more uniformly distributed along the apico-basal axis (Fig. 1). None of these organelles had a polarized distribution in E8 stage intestinal cells (Fig. 2), indicating that the cytoplasm undergoes a significant reorganization during epithelial polarization.

Epithelial polarization of *C. elegans* intestinal cells is controlled by PAR-3, which regulates multiple aspects of cortical polarization, including formation of an apically localized MTOC and the organization of apical cell-cell junctions (Achilleos et al., 2010; Feldman and Priess, 2012). However, unlike its roles at the cell cortex, PAR-3 is not required to generate asymmetries in organelle position along the apico-basal axis at the time of epithelial polarization (Fig. 3). This is in contrast to the requirement for PAR-3 in the apical positioning of endosomes in adult *C. elegans* intestinal cells (Winter et al., 2012), indicating that PAR-3 is necessary for the maintenance but not establishment of asymmetric organelle positioning in intestinal cells. In the *C. elegans* zygote PAR-3 directs the asymmetric positioning of early endosomes (Andrews and Ahringer, 2007), whereas PAR-3 is not required for asymmetric localization of early endosomes in polarizing intestinal cells (Fig. 3), highlighting the different mechanisms used to position organelles during development.

The non-random, asymmetric positioning of organelles along the apico-basal axis suggest active mechanisms control organelle localization. What then are the functional consequences of the constellation of organelle asymmetries created during epithelial polarization? The close association of conventional endolysosomal organelles with the nascent apical cell cortex might support membrane trafficking pathways known to establish and maintain epithelial polarity (Apodaca et al., 2012; Eaton and Martin-Belmonte, 2014; Mellman and Nelson, 2008). The apical migration of nuclei could act to restrict the interactions between apically and basally positioned organelles, similar to how the perinuclear cloud of endosomes in non-epithelial cells is segregated from peripheral organelles (Neefjes et al., 2017). The three basally enriched organelles, gut granules, yolk platelets, and lipid droplets, function in different aspects of lipid metabolism (Srinivasan, 2015; Watts and Ristow, 2017). It is therefore possible that being restricted to the same region of the cytoplasm facilitates exchange between similarly positioned organelles.

5.2. Mechanisms directing gut granule positioning

The asymmetric distribution of basally enriched gut granules and yolk platelets was disrupted in *unc-83*(–) mutants (Fig. 1). UNC-83 is a nuclear envelope localized KASH subunit of the conserved LINC complex (Starr et al., 2001), which contributes to the apical migration of nuclei during intestinal cell polarization by coupling nuclei to the cytoskeleton (Starr et al., 2001; Starr, 2019; Wong et al., 2021). Nuclei become centrally positioned within polarizing intestinal cells when UNC-83 function is disrupted (Fig. 1) (Starr et al., 2001), which likely explains how *unc-83*(–) disrupts apico-basal organelle asymmetry. This is in contrast to another *C. elegans* KASH protein ANC-1, which alters ER, mitochondrial, and lipid droplet positioning in hypodermal cells independently of its role in nuclear anchoring (Hao et al., 2021). During the polarization of intestinal cells, gut nuclei occupy a significant portion of the cytoplasm and when positioned near the midline likely contributes to basal organelle localization by excluding organelles from the apical domain. Gut granule and yolk platelet apico-basal polarity is lost and they gain access to the apical domain when nuclear positioning is disrupted. Notably, lipid droplets remain basally localized in *unc-83*(–) mutants (Fig. 1), indicating that their distribution is mediated by a different process. This could result from active basal transport, by forming stable contacts with basally anchored organelles, or by becoming clustered after being basally positioned so that they cannot pass nuclei (Kilwein and Welte, 2019; Olzmann and Carvalho, 2019). Endosomes and endolysosomes remain apically positioned when nuclear migration is disrupted. *unc-83*(–) does not obviously disrupt the apical MTOC or organization of the microtubule array (Feldman and Priess, 2012), and based on the

well-documented role of microtubules in endosome motility in other cell types (Rodriguez-Boulan and Macara, 2014; Leung et al., 1999; Neefjes et al., 2017; Bornens, 2008; Cabukusta and Neefjes, 2018), apico-basally oriented microtubules likely contribute to the positioning of apical endosomes during epithelial polarization.

The loss of gut granule apico-basal polarity in *wht-2*(–) is consistent with gut granule localization being the result of random diffusion and exclusion from the apical domain due to nuclear position. However, if passive mechanisms position gut granules, then we would not expect alterations in gut granule protein and lipid composition to disrupt their apico-basal polarization. It is therefore notable that mutations in BLOC-1 and HOPS complex subunits, which have conserved functions in LRO protein trafficking (Hermann et al., 2012; Delahaye et al., 2014), disrupted apico-basal gut granule polarity, without altering nuclear positioning (Fig. 7). Little is known regarding the role of LRO biogenesis factors in LRO positioning, likely because most LROs that have been studied to date do not exhibit asymmetric positioning similar to gut granules. However, the LRO biogenesis complexes HOPS and BLOC-3 promote the proper positioning of conventional lysosomes (Falcon-Perez et al., 2005; Galmes et al., 2015), albeit via unknown mechanisms. Regardless of whether BLOC-1 and HOPS directly control LRO motility or indirectly act to deliver cargo to gut granules that function in their positioning, their involvement in gut granule localization strongly suggests that gut granules are actively positioned basally along with being excluded from the apical domain by nuclei.

Our work shows that *wht-2* and *wht-7* have essential roles in gut granule positioning. However, unlike BLOC-1 and HOPS mutants, which no longer show apico-basal polarization of gut granules (Fig. 7), *wht-2*(–) and *wht-7*(–) mutants show a complete and specific reversal of gut granule positional asymmetry (Fig. 4), suggesting that WHT-2 and WHT-7 function differently than canonical trafficking factors.

wht-2 and *wht-7* encode WHT/ABCG half-transporters that are part of the White subfamily of ABC proteins, which actively translocate a diverse array of substrates across cellular membranes (Sheps et al., 2004). While ABCG transporters can function as homodimers (Tarr et al., 2009), our genetic experiments point to WHT-2/WHT-7 heterodimers controlling gut granule apico-basal polarity. Consistent with WHT-2 and WHT-7 acting together, the *wht-2*(–) and *wht-7*(–) single and *wht-2*(–); *wht-7*(–) double mutants showed identical effects on gut granule positioning (Fig. 9). While the single mutants had little effect on gut granule positioning, combining WHT-2 and WHT-7 Walker A motif ATPase mutants led to the apical enrichment of gut granules (Fig. 10). Due to the composite nature of ATP binding sites created by each subunit when ABCG proteins dimerize (Eckenstaler and Benndorf, 2020), this result strongly suggests that WHT-2 and WHT-7 function as a heterodimer. If WHT-2 and WHT-7 act as homodimers to direct gut granule localization, then disrupting their ATPase activity should alter gut granule positioning similar to the deletion mutants, which they did not (Fig. 10) (Eckenstaler and Benndorf, 2020).

There is precedent for individual ABCG transporters functioning as heterodimers as well as homodimers (Kerr et al., 2011). Our analysis of *wht-2*(–) and *wht-7*(–) single mutants indicates that WHT-2 has WHT-7 independent functions in gut granule biogenesis. Whereas *wht-2*(–) disrupts the formation of crystalline gut granule contents (Fig. 9), exhibits genetic interactions with *glo-3*(–) (Voss et al., 2020), and leads to the loss of the GLO-1 Rab from gut granules (Fig. 11), *wht-7*(–) does not have any of these effect (Figs. 9, 11, S2). Moreover, WHT-2 is trafficked to gut granules in the absence of WHT-7 (Fig. 9), where it could function independently of WHT-7. We therefore propose that WHT-2 acts as a homodimer in gut granule biogenesis and as part of a WHT-2/WHT-7 heterodimer in gut granule positioning.

The significant apical enrichment of gut granules in WHT-2(K74R); WHT-7(K105R) Walker A motif mutants strongly suggests that WHT-2 and WHT-7 function as a membrane transporter in gut granule positioning (Fig. 10). ABCG transporters bind substrates at the interface between the monomers (Banerjee et al., 2021), suggesting the possibility

that WHT-2 transporter specificity is altered by whether it homo or heterodimerizes. This would be similar to the *Drosophila* ABCG protein White, which has been proposed to transport different substrates into lysosome-related pigment granules depending upon whether it heterodimerizes with Scarlet or Brown (Mackenzie et al., 2000). While the substrates transported by WHT-2/WHT-7 impacting gut granule positioning are unknown, homologous human ABCG transporters transport a variety of lipids (Neumann et al., 2017), which are known to be key drivers of cell polarity due to their effects on membrane architecture (Vaidziulyte et al., 2019). Additionally, changes in membrane lipid composition can directly impact microtubule motor function to alter organelle position (Roney et al., 2021).

When gut granule protein trafficking is disrupted by mutations in subunits of the BLOC-1 (*glo-2*), BLOC-3-like (*glo-3*), and HOPS (*vps-18*) complexes (Bowman et al., 2019), some gut granules became localized apically, but not to the same levels as seen in *wht-2(–)* and *wht-7(–)* mutants (Fig. 7). Moreover, *wht-2(–)* and *wht-7(–)* mutants did not show any defects in the localization of gut granule proteins and their gut granules did not take on any of the characteristics of apically localized conventional endosomes (Figs. 6 and 9). This suggests that the *wht* mutants do not generally alter gut granule formation to cause their mispositioning.

Altering the lipid composition of lysosomal membranes can promote lysophagy, the targeting and destruction of lysosomes by autophagy (Papadopoulos and Meyer, 2017). Disrupted WHT-2/WHT-7 transporter activity could similarly change gut granule membranes, leading to their clearance. If gut granules were placed within autophagosomes they could be targeted apically in order to fuse with conventional lysosomes and be degraded. However, gut granules are abundant in later stage embryos (Voss et al., 2020) and RAB-7, which associates with autophagosomes (Lorincz and Juhasz, 2020), was not detected on gut granules in *wht-2(–)* mutants (Fig. 6). We therefore think it likely that WHT-2 and WHT-7 affect a specific process impacting gut granule positioning rather than generally altering gut granule formation or causing their degradation in apical endolysosomes.

5.3. WHT-2 controls gut granule positioning through Rabs

The phenotypes of *wht-2(–)* and *wht-7(–)* loss-of-function mutants indicate that WHT-2/WHT-7 functions to prevent the apical accumulation of gut granules. During epithelial polarization, gut granules, like early endosomes and endolysosomes, might contain factors with the potential to promote their apical positioning. In this scenario, WHT-2/WHT-7 could be directly or indirectly inhibiting these factors and/or promoting the activity of factors directing gut granules basally. Alternatively, gut granules might lack factors directing apico-basal positioning and when WHT-2/WHT-7 activity is disrupted, they acquire a factor mediating their apical localization.

Our studies suggest that GLO-1, a Rab32/38 homolog (Hermann et al., 2005), acts downstream of WHT-2/WHT-7 to direct the polarized distribution of gut granules. Strikingly, ectopic expression of GLO-1 led to the restoration of basal gut granules in *wht-2(–)* and *wht-7(–)* mutants and the targeted degradation of GLO-1 led to the apical accumulation of gut granules (Figs. 12 and 13). In addition, the loss of GLO-1 from gut granules immediately preceded their apical mispositioning in *wht-2(–)* mutants (Fig. 11). Vertebrate Rab32/38 functions in LRO motility and physically interacts with myosin (Park et al., 2007; Bultema et al., 2014; Hume et al., 2011), supporting the possibility that GLO-1 directs the basal localization of gut granules.

GLO-3 is a subunit of the likely GLO-1 activating guanine nucleotide exchange factor (GEF) and gut granules in *glo-3(kx38)*, like *wht-2(–)* mutants, lack GLO-1 (Morris et al., 2018). If gut granule associated GLO-1 functions in gut granule positioning, then why do gut granules not become apically enriched in *glo-3(–)* mutants (Fig. 7)? We believe that the different functions of WHT-2 and GLO-3 in GLO-1 activation and gut granule biogenesis could explain their different roles in gut granule

positioning. Inactive GLO-1(GDP) likely accumulates when GLO-3/GEF activity is disrupted, whereas WHT-2 has a GEF independent role in the association of GLO-1 with gut granules (Voss et al., 2020). The loss of active GLO-1(GTP) disrupts gut granule biogenesis, resulting in *glo-3(–)* mutants having significant alterations in gut granule protein composition, a phenotype not displayed by *wht-2(–)* (Voss et al., 2020). It is therefore possible that defects in gut granule biogenesis caused by *glo-3(–)* produce gut granules lacking factors promoting their apical accumulation. These factors would be present when WHT-2 function is disrupted due to a more limited role of WHT-2 in gut granule biogenesis. Consistent with this idea, WHT-2 does not appear to impact GLO-1 localization to gut granules until the E16 stage (Fig. 11), which is after the initiation of gut granule biogenesis (Voss et al., 2020). If the GLO-1 Rab regulates gut granule biogenesis in E8 and earlier stage intestinal cells before transitioning to regulating gut granule positioning at the E16 stage, then *wht-2(–)* could specifically impact GLO-1 function in organelle localization during epithelial polarization.

Our data support the model that WHT-2 promotes the localization of GLO-1 to E16 stage gut granules, which in turn prevents their apical localization. Our results also point to WHT-2 functioning as a membrane transporter with WHT-7 to position gut granules (Figs. 10 and 12). It is therefore surprising that *wht-7(–)* does not cause the loss of GLO-1 from E16 gut granules, in contrast to *wht-2(–)* (Fig. 11). It is important to note that we analyzed the steady state localization of GLO-1, leaving open the possibility that *wht-7(–)* is altering dynamics of GLO-1 localization that are important to its activity. For example, there might be an increased rate of GLO-1 cycling on and off gut granules, decreasing the duration of GLO-1 association, either of which could impact GLO-1 function. Alternatively, *wht-7(–)* might not disrupt the association of GLO-1 with gut granules, but instead lead to decreased nucleotide exchange and activation of GLO-1. In either scenario WHT-2 homodimers might partially compensate for the loss of WHT-7 to support the steady state localization of GLO-1 in *wht-7(–)*. It is important to note that our data do not exclude the possibility that WHT-7 acts independently of WHT-2 and GLO-1 to impact gut granule positioning. However, this seems unlikely in light of the synthetic genetic interactions between WHT-2 and WHT-7 ATPase mutants and the suppression of both *wht-2(–)* and *wht-7(–)* by the ectopic expression of GLO-1 (Figs. 10 and 12).

Our work also points to a role for the endolysosomal RAB-7 in gut granule mispositioning. When WHT-2 or GLO-1 activity was disrupted, *rab-7(RNAi)* potently suppressed the apical mislocalization of gut granules (Figs. 7 and 13). While not as strong, *rab-7(RNAi)* also suppressed *wht-7(–)* (Fig. 7). Interestingly, when GLO-1 was targeted for degradation, RAB-7 became associated with some apically mispositioned gut granules (Fig. 13). Rab7 is known to mediate the bidirectional transport of endolysosomes along microtubules through its recruitment of kinesin and dynein (Cabukusta and Neefjes, 2018; Pu et al., 2016), suggesting the possibility that mislocalized RAB-7 could direct the apical directed movement of gut granules along the polarized microtubule array that is present in E16 stage intestinal cells (Leung et al., 1999).

The asymmetries in organelle positioning associated with epithelial polarization have rarely been documented and are largely unexplored. Polarizing *C. elegans* intestinal cells represent an attractive system to investigate the mechanisms that generate, and the consequences of, organelle asymmetries. While our studies of WHT-2/WHT-7 and the GLO-1 and RAB-7 GTPases provide insights into asymmetric gut granule positioning, the mechanisms directing the apical accumulation of conventional endosomes and the basal localization of lipid droplets in polarizing epithelial cells are currently unknown and warrant further study.

Acknowledgements

We thank Jon Audhya, Barth Grant, Kerry Kornfeld, Fritz Mueller, Jeremy Nance, and Xiochen Wang for strains and antibodies. We thank members of the Hermann lab, Margaret Metz, Deborah Lycan, and

Tamily Weissman for helpful discussions. We are grateful to Nicole Brockway for assistance with confocal microscopy. We thank Gillian Beran-Maryott, Lucien Childs-Mitchell, Caroline Devincenzi, Alex Gustavson, Alex MacColl Garfinkle, Tessa Marzulla, Riley Mitchell, Hannah Somhegyi, Christine Van Tubbergen, and Andrew Wood, student in the 2011 edition of Bio412, for making the initial observations that led to this study. Some of the strains used in this work were provided by the *Caenorhabditis* Genetics Center and the National Bioresource Project for *Caenorhabditis elegans*. This work was supported by the National Institutes of Health (1R15GM120639-01), the National Science Foundation (MCB1612804), the Howard Hughes Medical Institute, and the John S. Rogers Summer Research Program.

Appendix A. Supplementary data

Supplementary data to this article can be found online at <https://doi.org/10.1016/j.ydbio.2021.09.007>.

References

Achilleos, A., Wehman, A.M., Nance, J., 2010. PAR-3 mediates the initial clustering and apical localization of junction and polarity proteins during *C. elegans* intestinal epithelial cell polarization. *Development* 137 (11), 1833–1842.

Andrews, R., Ahringer, J., 2007. Asymmetry of early endosome distribution in *C. elegans* embryos. *PLoS One* 2 (6), e493.

Apodaca, G., Gallo, L.I., Bryant, D.M., 2012. Role of membrane traffic in the generation of epithelial cell asymmetry. *Nat Cell Biol* 14 (12), 1235–1243.

Audhya, A., Desai, A., Oegema, K., 2007. A role for Rab5 in structuring the endoplasmic reticulum. *J. Cell Biol.* 178 (1), 43–56.

Ballabio, A., Bonifacino, J.S., 2020. Lysosomes as dynamic regulators of cell and organismal homeostasis. *Nat Rev Mol Cell Biol* 21 (2), 101–118.

Banerjee, A., Moreno, A., Pata, J., Falson, P., Prasad, R., 2021. ABCG: a new fold of ABC exporters and a whole new bag of riddles! *Adv Protein Chem Struct Biol* 123, 163–191.

Bone, C.R., Starr, D.A., 2016. Nuclear migration events throughout development. *Journal of Cell Science* 129 (10), 1951–1961.

Bornens, M., 2008. Organelle positioning and cell polarity. *Nat Rev Mol Cell Biol* 9 (11), 874–886.

Bowman, S.L., Bi-Karchin, J., Le, L., Marks, M.S., 2019. The road to LROs: insights into lysosome-related organelles from Hermansky-Pudlak syndrome and other rare diseases. *Traffic* 20, 404–435.

Bultema, J.J., Boyle, J.A., Malenke, P.B., Martin, F.E., Dell'Angelica, E.C., Cheney, R.E., Di Pietro, S.M., 2014. Myosin Vc interacts with Rab32 and Rab38 proteins and works in the biogenesis and secretion of melanosomes. *Journal of Biological Chemistry* 289 (48), 33513–33528.

Burakov, A.V., Nadezhina, E.S., 2013. Association of nucleus and centrosome: magnet or velcro? *Cell Biol Int* 37 (2), 95–104.

Cabukusta, B., Neefjes, J., 2018. Mechanisms of lysosomal positioning and movement. *Traffic* 19 (10), 761–769.

Chen, C.C., Schweihsberg, P.J., Vashist, S., Mareiniss, D.P., Lambie, E.J., Grant, B.D., 2006. RAB-10 is required for endocytic recycling in the *Caenorhabditis elegans* intestine. *Mol. Biol. Cell* 17 (3), 1286–1297.

Chen, B., Jiang, Y., Zeng, S., Yan, J., Li, X., Zhang, Y., Zou, W., Wang, X., 2010. Endocytic sorting and recycling require membrane phosphatidylserine asymmetry maintained by TAT-1/CHAT-1. *PLOS Genet* 6 (12), e1001235.

Cseres, J., Szentpetery, Z., Seres, L., Ozvegy-Laczka, C., Langmann, T., Schmitz, G., Glavinas, H., Klein, I., Homolya, L., Varadi, A., Sarkadi, B., Elkind, N.B., 2004. Functional expression and characterization of the human ABCG1 and ABCG4 proteins: indications for heterodimerization. *Biochem Biophys Res Commun* 320 (3), 860–867.

Davis, D.E., Roh, H.C., Deshmukh, K., Bruinsma, J.J., Schneider, D.L., Guthrie, J., Robertson, J.D., Kornfeld, K., 2009. The cation diffusion facilitator gene *cdf-2* mediates zinc metabolism in *Caenorhabditis elegans*. *Genetics* 182 (4), 1015–1033.

Delahaye, J.L., Foster, O.K., Vine, A., Saxton, D.S., Curtin, T.P., Somhegyi, H., Salesky, R., Hermann, G.J., 2014. *Caenorhabditis elegans* HOPS and CCZ-1 mediate trafficking to lysosome-related organelles independently of RAB-7 and SAND-1. *Mol Biol Cell* 25 (7), 1073–1096.

Dumas, J.J., Merithew, E., Sudharshan, E., Rajamani, D., Hayes, S., Lawe, D., Corvera, S., Lambright, D.G., 2001. Multivalent endosome targeting by homodimeric EEA1. *Mol Cell* 8 (5), 947–958.

Eaton, S., Martin-Belmonte, F., 2014. Cargo sorting in the endocytic pathway: a key regulator of cell polarity and tissue dynamics. *Cold Spring Harb Perspect Biol* 6 (10), a016899.

Eckenstaler, R., Benndorf, R.A., 2020. 3D structure of the transporter ABCG2-What's new? *Br J Pharmacol* 177 (7), 1485–1496.

Eisenhut, R.J., Knox, D., Hermann, G.J., 2005. Characterization of a conserved apoptotic marker expressed in *Caenorhabditis elegans* phagocytic cells. *Biochem Biophys Res Commun* 335 (4), 1231–1238.

Falcon-Perez, J.M., Nazarian, R., Sabatti, C., Dell'Angelica, E.C., 2005. Distribution and dynamics of Lamp1-containing endocytic organelles in fibroblasts deficient in BLOC-3. *J Cell Sci* 118 (Pt 22), 5243–5255.

Feldman, J.L., Priess, J.R., 2012. A role for the centrosome and PAR-3 in the hand-off of MTOC function during epithelial polarization. *Curr Biol* 22 (7), 575–582.

Fridolfsson, H.N., Herrera, L.A., Brandt, J.N., Cain, N.E., Hermann, G.J., Starr, D.A., 2018. Genetic analysis of nuclear migration and anchorage to study LINC complexes during development of *Caenorhabditis elegans*. In: *The LINC Complexes: Methods and Protocols*. Springer, pp. 163–180.

Galmes, R., ten Brink, C., Oorschot, V., Veenendaal, T., Jonker, C., van der Sluijs, P., Klumperman, J., 2015. Vps33B is required for delivery of endocytosed cargo to lysosomes. *Traffic* 16 (12), 1288–1305.

Gao, M., Cui, H.R., Loe, D.W., Grant, C.E., Almquist, K.C., Cole, S.P.C., Deeley, R.G., 2000. Comparison of the functional characteristics of the nucleotide binding domains of multidrug resistance protein 1. *Journal of Biological Chemistry* 275 (17), 13098–13108.

Hadwiger, G., Dour, S., Arur, S., Fox, P., Nonet, M.L., 2010. A monoclonal antibody toolkit for *C. elegans*. *PLOS One* 5 (4), e10161.

Hao, H., Kalra, S., Jameson, L.E., Guerrero, L.A., Cain, N.E., Bolivar, J., Starr, D.A., 2021. The Nesprin-1/2 ortholog ANC-1 regulates organelle positioning in *C. elegans* independently from its KASH or actin-binding domains. *Elife* 10.

Hegyi, Z., Homolya, L., 2016. Functional cooperativity between ABCG4 and ABCG1 isoforms. *Plos One* 11 (5).

Henriksen, U., Gether, U., Litman, T., 2005. Effect of Walker A mutation (K86M) on oligomerization and surface targeting of the multidrug resistance transporter ABCG2. *J Cell Sci* 118 (Pt 7), 1417–1426.

Hermann, G.J., Schroeder, L.K., Hieb, C.A., Kershner, A.M., Rabitts, B.M., Fonarev, P., Grant, B.D., Priess, J.R., 2005. Genetic analysis of lysosomal trafficking in *Caenorhabditis elegans*. *Mol. Biol. Cell* 16 (7), 3273–3288.

Hermann, G.J., Scavarda, E., Weis, A.M., Saxton, D.S., Thomas, L.L., Salesky, R., Somhegyi, H., Curtin, T.P., Barrett, A., Foster, O.K., Vine, A., Erlich, K., Kwan, E., Rabitts, B.M., Warren, K., 2012. *C. elegans* BLOC-1 functions in trafficking to lysosome-related gut granules. *PLoS One* 7 (8), e43043.

Hume, A.N., Wilson, M.S., Ushakov, D.S., Ferenczi, M.A., Seabra, M.C., 2011. Semi-automated analysis of organelle movement and membrane content: understanding rab-motor complex transport function. *Traffic* 12 (12), 1686–1701.

Kamat, R.S., Martinez-Campos, M., Zipperlen, P., Fraser, A.G., Ahringer, J., 2001. Effectiveness of specific RNA-mediated interference through ingested double-stranded RNA in *Caenorhabditis elegans*. *Genome Biol* 2 (1). RESEARCH0002.

Kemphues, K.J., Priess, J.R., Morton, D.G., Cheng, N., 1988. Identification of genes required for cytoplasmic localization in the early *C. elegans* embryos. *Cell* 52, 311–320.

Kerr, I.D., Haider, A.J., Gelissen, I.C., 2011. The ABCG family of membrane-associated transporters: you don't have to be big to be mighty. *Br J Pharmacol* 164 (7), 1767–1779.

Khatter, D., Sindhwan, A., Sharma, M., 2015. Arf-like GTPase Arl8: moving from the periphery to the center of lysosomal biology. *Cell Logist* 5 (3), e1086501.

Kilwein, M.D., Welte, M.A., 2019. Lipid Droplet Motility and Organelle Contacts. *Contact*, vol. 2. Thousand Oaks).

Kummel, D., Ungermann, C., 2014. Principles of membrane tethering and fusion in endosome and lysosome biogenesis. *Curr Opin Cell Biol* 29C, 61–66.

Lang, C.F., Munro, E., 2017. The PAR proteins: from molecular circuits to dynamic self-stabilizing cell polarity. *Development* 144 (19), 3405–3416.

Leung, B., Hermann, G.J., Priess, J.R., 1999. Organogenesis of the *Caenorhabditis elegans* intestine. *Dev. Biol.* 216 (1), 114–134.

Levitte, S., Salesky, R., King, B., Coe Smith, S., Depper, M., Cole, M., Hermann, G.J., 2010. A *Caenorhabditis elegans* model of orotic aciduria reveals enlarged lysosome-related organelles in embryos lacking *umps-1* function. *FEBS J* 277 (6), 1420–1439.

Liu, F., Thatcher, J.D., Barral, J.M., Epstein, H.F., 1995. Bifunctional glyoxylate cycle protein of *Caenorhabditis elegans*: a developmentally regulated protein of intestine and muscle. *Dev Biol* 169 (2), 399–414.

Liu, B., Du, H., Rutkowski, R., Gartner, A., Wang, X., 2012. LAAT-1 is the lysosomal lysine/arginine transporter that maintains amino acid homeostasis. *Science* 337 (6092), 351–354.

Lorincz, P., Juhasz, G., 2020. Autophagosome-lysosome fusion. *J Mol Biol* 432 (8), 2462–2482.

Mackenzie, S.M., Howells, A.J., Cox, G.B., Ewart, G.D., 2000. Sub-cellular localization of the White/Scarlet ABC transporter to pigment granule membranes within the compound eye of *Drosophila melanogaster*. *Genetica* 108, 239–252.

Maduro, M.F., 2017. Gut development in *C. elegans*. *Semin Cell Dev Biol* 66, 3–11.

Mellman, I., Nelson, W.J., 2008. Coordinated protein sorting, targeting and distribution in polarized cells. *Nat Rev Mol Cell Biol* 9 (11), 833–845.

Moorthy, S., Chen, L., Bennet, V., 2000. *Caenorhabditis elegans* beta-G spectrin is dispensable for the establishment of epithelial polarity, but essential for muscular and neuronal function. *J. Cell. Biol.* 149, 915–930.

Morris, C., Foster, O.K., Handa, S., Pelozza, K., Voss, L., Somhegyi, H., Jian, Y., Vo, M.V., Harp, M., Rambo, F.M., Yang, C., Hermann, G.J., 2018. Function and regulation of the *Caenorhabditis elegans* Rab32 family member GLO-1 in lysosome-related organelle biogenesis. *PLoS Genet* 14 (11), e1007772.

Nakae, I., Fujino, T., Kobayashi, T., Sasaki, A., Kikkawa, Y., Fukuyama, M., Gengyo-Ando, K., Mitani, S., Kontani, K., Katada, T., 2010. The arf-like GTPase Arl8 mediates delivery of endocytosed macromolecules to lysosomes in *Caenorhabditis elegans*. *Mol Biol Cell* 21 (14), 2434–2442.

Nance, J., Munro, E.M., Priess, J.R., 2003. *C. elegans* PAR-3 and PAR-6 are required for apicobasal asymmetries associated with cell adhesion and gastrulation. *Development* 130 (22), 5339–5350.

Neefjes, J., Jongsma, M.M.L., Berlin, I., 2017. Stop or go? Endosome positioning in the establishment of compartment architecture, dynamics, and function. *Trends Cell Biol* 27 (8), 580–594.

Neukomm, L.J., Nicot, A.S., Kinchen, J.M., Almendinger, J., Pinto, S.M., Zeng, S., Doukoumetzidis, K., Tronchere, H., Payrastre, B., Laporte, J.F., Hengartner, M.O., 2011. The phosphoinositide phosphatase MTM-1 regulates apoptotic cell corpse clearance through CED-5-CED-12 in *C. elegans*. *Development* 138 (10), 2003–2014.

Neumann, J., Rose-Sperling, D., Hellmich, U.A., 2017. Diverse relations between ABC transporters and lipids: an overview. *Biochim Biophys Acta Biomembr* 1859 (4), 605–618.

Olzmann, J.A., Carvalho, P., 2019. Dynamics and functions of lipid droplets. *Nat Rev Mol Cell Biol* 20 (3), 137–155.

Ozvegy, C., Varadi, A., Sarkadi, B., 2002. Characterization of drug transport, ATP hydrolysis, and nucleotide trapping by the human ABCG2 multidrug transporter. Modulation of substrate specificity by a point mutation. *J Biol Chem* 277 (50), 47980–47990.

Papadopoulos, C., Meyer, H., 2017. Detection and clearance of damaged lysosomes by the endo-lysosomal damage response and lysophagy. *Curr Biol* 27 (24), R1330–R1341.

Park, M., Serpinskaya, A.S., Papalopulu, N., Gelfand, V.I., 2007. Rab32 regulates melanosome transport in *Xenopus* melanophores by protein kinase A recruitment. *Curr Biol* 17 (23), 2030–2034.

Perria, C.L., Rajamanickam, V., Lapinski, P.E., Raghavan, M., 2006. Catalytic site modifications of TAP1 and TAP2 and their functional consequences. *Journal of Biological Chemistry* 281 (52), 39839–39851.

Pickett, M.A., Naturale, V.F., Feldman, J.L., 2019. A polarizing issue: diversity in the mechanisms underlying apico-basolateral polarization in vivo. *Annu Rev Cell Dev Biol* 35, 285–308.

Procko, E., Ferrin-O'Connell, I., Ng, S.L., Gaudet, R., 2006. Distinct structural and functional properties of the ATPase sites in an asymmetric ABC transporter. *Molecular Cell* 24 (1), 51–62.

Pu, J., Guardia, C.M., Keren-Kaplan, T., Bonifacino, J.S., 2016. Mechanisms and functions of lysosome positioning. *Journal of Cell Science* 129 (23), 4329–4339.

Rabbitts, B.M., Kokes, M., Miller, N.E., Kramer, M., Lawrenson, A.L., Levitte, S., Kremer, S., Kwan, E., Weis, A.M., Hermann, G.J., 2008. *glo-3*, a novel *Caenorhabditis elegans* gene, is required for lysosome-related organelle biogenesis. *Genetics* 180, 857–871.

Riga, A., Castiglioni, V.G., Boxem, M., 2020. New insights into apical-basal polarization in epithelia. *Curr Opin Cell Biol* 62, 1–8.

Rizk, A., Paul, G., Incardona, P., Bugarski, M., Mansouri, M., Niemann, A., Ziegler, U., Berger, P., Sbalzarini, I.F., 2014. Segmentation and quantification of subcellular structures in fluorescence microscopy images using Squash. *Nat Protoc* 9 (3), 586–596.

Rodriguez-Boulan, E., Macara, I.G., 2014. Organization and execution of the epithelial polarity programme. *Nat Rev Mol Cell Biol* 15 (4), 225–242.

Roman-Fernandez, A., Bryant, D.M., 2016. Complex polarity: building multicellular tissues through apical membrane traffic. *Traffic* 17 (12), 1244–1261.

Roney, J.C., Li, S., Farfel-Becker, T., Huang, N., Sun, T., Xie, Y., Cheng, X.T., Lin, M.Y., Platt, F.M., Sheng, Z.H., 2021. Lipid-mediated motor-adaptor sequestration impairs axonal lysosome delivery leading to autophagic stress and dystrophy in Niemann-Pick type C. *Dev Cell* 56 (in press).

Sarkadi, B., Homolya, L., Szakacs, G., Varadi, A., 2006. Human multidrug resistance ABCB and ABCG transporters: participation in a chemoimmunity defense system. *Physiol Rev* 86 (4), 1179–1236.

Sato, M., Sato, K., Fonarev, P., Huang, C.J., Liou, W., Grant, B.D., 2005. *Caenorhabditis elegans* RME-6 is a novel regulator of RAB-5 at the clathrin-coated pit. *Nat Cell Biol* 7 (6), 559–569.

Sato, K., Norris, A., Sato, M., Grant, B.D., 2014. *C. elegans* as a model for membrane traffic (April 25, 2014). In: *Wormbook*, T.C.E.R. (Ed.), *Wormbook*. Wormbook.

Schindelin, J., Arganda-Carreras, I., Frise, E., Kaynig, V., Longair, M., Pietzsch, T., Preibisch, S., Rueden, C., Saalfeld, S., Schmid, B., Tinevez, J.Y., White, D.J., Hartenstein, V., Eliceiri, K., Tomancak, P., Cardona, A., 2012. Fiji: an open-source platform for biological-image analysis. *Nat Methods* 9 (7), 676–682.

Schroeder, L.K., Kremer, S., Kramer, M.J., Currie, E., Kwan, E., Watts, J.L., Lawrenson, A.L., Hermann, G.J., 2007. Function of the *Caenorhabditis elegans* ABC transporter PGP-2 in the biogenesis of a lysosome-related fat storage organelle. *Mol Biol Cell* 18 (3), 995–1008.

Scott, C.C., Vacca, F., Gruenberg, J., 2014. Endosome maturation, transport and functions. *Semin Cell Dev Biol* 31, 2–10.

Sheps, J.A., Ralph, S., Zhao, Z., Baillie, D.L., Ling, V., 2004. The ABC transporter gene family of *Caenorhabditis elegans* has implications for the evolutionary dynamics of multidrug resistance in eukaryotes. *Genome Biol* 5 (3), R15.

Simons, K., Fuller, S.D., 1985. Cell surface polarity in epithelia. *Annu Rev Cell Biol* 1, 243–288.

Srinivasan, S., 2015. Regulation of body fat in *Caenorhabditis elegans*. *Annu Rev Physiol* 77, 161–178.

Starr, D.A., 2019. A network of nuclear envelope proteins and cytoskeletal force generators mediates movements of and within nuclei throughout *Caenorhabditis elegans* development. *Exp Biol Med (Maywood)* 244 (15), 1323–1332.

Starr, D.A., Hermann, G.J., Malone, C.J., Fixsen, W., Priess, J.R., Horvitz, H.R., Han, M., 2001. *unc-83* encodes a novel component of the nuclear envelope and is essential for proper nuclear migration. *Development* 128, 5039–5050.

Stiernagle, T., 1999. Maintenance of *C. elegans*. In: Hope, I. (Ed.), *C. elegans: A Practical Approach*. Oxford University Press, pp. 51–67.

Sulston, J.E., 1976. Post-embryonic development in the ventral cord of *Caenorhabditis elegans*. *Philos. Trans. R. Soc. Lond. B. Biol. Sci.* 275, 287–297.

Tarr, P.T., Tarling, E.J., Bojanic, D.D., Edwards, P.A., Baldan, A., 2009. Emerging new paradigms for ABCG transporters. *Biochim Biophys Acta* 1791 (7), 584–593.

Taverna, E., Gotz, M., Huttner, W.B., 2014. The cell biology of neurogenesis: toward an understanding of the development and evolution of the neocortex. *Annu Rev Cell Dev Biol* 30, 465–502.

Taylor, N.M.I., Manolari, I., Jackson, S.M., Kowal, J., Stahlberg, H., Locher, K.P., 2017. Structure of the human multidrug transporter ABCG2. *Nature* 546 (7659), 504–509.

Thompson, O., Edgley, M., Strasbourger, P., Flibotte, S., Ewing, B., Adair, R., Au, V., Chaudhry, I., Fernando, L., Hutter, H., Kieffer, A., Lau, J., Lee, N., Miller, A., Raymant, G., Shen, B., Shendure, J., Taylor, J., Turner, E.H., Hillier, L.W., Moerman, D.G., Waterston, R.H., 2013. The million mutation project: a new approach to genetics in *Caenorhabditis elegans*. *Genome Res* 23 (10), 1749–1762.

Treusch, S., Knuth, S., Slaugenhaupt, S.A., Goldin, E., Grant, B.D., Fares, H., 2004. *Caenorhabditis elegans* functional orthologue of human protein h-mucolipin-1 is required for lysosome biogenesis. *Proc. Natl. Acad. Sci. (USA)* 13, 4483–4488.

Trivedi, P.C., Bartlett, J.J., Pulinilkunnil, T., 2020. Lysosomal biology and function: modern view of cellular debris bin. *Cells* 9 (5).

Vaidziulyte, K., Coppey, M., Schauer, K., 2019. Intracellular organization in cell polarity - placing organelles into the polarity loop. *J Cell Sci* 132 (24).

Voss, L., Foster, O.K., Harper, L., Morris, C., Lavoy, S., Brandt, J.N., Peloza, K., Handa, S., Maxfield, A., Harp, M., King, B., Eichten, V., Rambo, F.M., Hermann, G.J., 2020. An ABCG transporter functions in Rab localization and lysosome-related organelle biogenesis in *Caenorhabditis elegans*. *Genetics* 214 (2), 419–445.

Wang, S., Tang, N.H., Lara-Gonzalez, P., Zhao, Z., Cheerambathur, D.K., Prevo, B., Chisholm, A.D., Desai, A., Oegema, K., 2017. A toolkit for GFP-mediated tissue-specific protein degradation in *C. elegans*. *Development* 144 (14), 2694–2701.

Watts, J.L., Ristow, M., 2017. Lipid and carbohydrate metabolism in *Caenorhabditis elegans*. *Genetics* 207 (2), 413–446.

Winter, J.F., Hopfner, S., Korn, K., Farnung, B.O., Bradshaw, C.R., Marsico, G., Volkmer, M., Habermann, B., Zerial, M., 2012. *Caenorhabditis elegans* screen reveals role of PAR-5 in RAB-11-recycling endosome positioning and apicobasal cell polarity. *Nat Cell Biol* 14 (7), 666–676.

Wong, X., Loo, T.H., Stewart, C.L., 2021. LINC complex regulation of genome organization and function. *Curr Opin Genet Dev* 67, 130–141.

Zhang, D.W., Graf, G.A., Gerard, R.D., Cohen, J.C., Hobbs, H.H., 2006. Functional asymmetry of nucleotide-binding domains in ABCG5 and ABCG8. *J Biol Chem* 281 (7), 4507–4516.

Zhang, S.O., Box, A.C., Xu, N., Le Men, J., Yu, J., Guo, F., Trimble, R., Mak, H.Y., 2010. Genetic and dietary regulation of lipid droplet expansion in *Caenorhabditis elegans*. *Proc Natl Acad Sci U S A* 107 (10), 4640–4645.

Zhang, H., Abraham, N., Khan, L.A., Hall, D.H., Fleming, J.T., Gobel, V., 2011. Apicobasal domain identities of expanding tubular membranes depend on glycosphingolipid biosynthesis. *Nat Cell Biol* 13 (10), 1189–1201.